Similarity in phytoplankton photophysiology among under-ice, marginal ice, and open water environments of Baffin Bay (Arctic Ocean)

Hannah L Joy-Warren, Kate M Lewis, Mathieu Ardyna, Jean-Éric Tremblay, Marcel Babin, Kevin R Arrigo

ELEMENTA
Science of the Anthropocene

Joy-Warren, H, et al. 2023. Similarity in phytoplankton photophysiology among under-ice, marginal ice, and open water environments of Baffin Bay (Arctic Ocean). *Elem Sci Anth*, 11: 1. DOI: https://doi.org/10.1525/elementa.2021.00080

RESEARCH ARTICLE

Similarity in phytoplankton photophysiology among under-ice, marginal ice, and open water environments of Baffin Bay (Arctic Ocean)

Hannah Joy-Warren[1,2,3,4,*], Kate M. Lewis[1], Mathieu Ardyna[1,5,6], Jean-Éric Tremblay[5], Marcel Babin[5], and Kevin R. Arrigo[1]

As sea ice is declining rapidly in the Arctic, phytoplankton are being exposed to very different light regimes. Here we investigated how phytoplankton photoacclimate in three different irradiance regimes: under the ice, in the marginal ice zone, and in open water. We sampled from these three regimes in spring–summer 2016 during the Green Edge cruise in Baffin Bay. We also conducted experiments to investigate the impact of short-term surface light exposure on phytoplankton photophysiology, focusing on processes related to photoprotection and photodamage. These experiments were designed to simulate phytoplankton mixing to the surface or sea ice rapidly disappearing. Despite differences in hydrography, nutrient concentrations, light conditions, and phytoplankton biomass in each regime, the phytoplankton community was similar in terms of photophysiological state. Photoprotective pigments (including the xanthophyll cycle) were high in all three regimes sampled. As with the in situ measurements, ice conditions and light history had little impact on how phytoplankton responded to the light shock, leading us to conclude that phytoplankton are largely prepared for a high light transition, even when originating from low light environments under sea ice.

Keywords: Phytoplankton photophysiology, Arctic Ocean, Marginal ice zone, Photoprotection, Photodamage

1. Introduction

Climate change is drastically altering Arctic ecosystems (Wassmann et al., 2011; Arctic Monitoring and Assessment Programme, 2017; Intergovernmental Panel on Climate Change, 2019). Sea ice is declining dramatically, both in extent and thickness (Comiso et al., 2008; Kwok, 2018; Stroeve and Notz, 2018), and the Arctic is predicted to be ice-free by the middle of this century (Stroeve et al., 2007; Wang and Overland, 2009). These changes in sea ice have important implications for Arctic ecosystems. Two important changes—the transition from multi-year ice to first-year ice (Kwok and Rothrock, 2009; Maslanik et al., 2011), as well as earlier sea ice melt and delayed freeze-up (Arrigo and van Dijken, 2011)—are increasing the light transmission to the underwater environment (Katlein et al., 2015; Katlein et al., 2019).

The reduction in sea ice may increase both the time period and the regions that are favorable for phytoplankton growth. Kahru et al. (2011) demonstrated that the spring phytoplankton bloom is occurring earlier in the season. Meanwhile, Ardyna et al. (2014) showed that delayed ice freeze-up, which allows for more wind-driven mixing and nutrient delivery (Mioduszewski et al., 2018), can increase the frequency of a second phytoplankton bloom, this one coming in the fall. Consistent with these findings, satellite data show that until around 2010, net primary production (NPP) in the Arctic Ocean increased due to greater open water area and a longer phytoplankton growing season (Arrigo et al., 2008; Pabi et al., 2008; Arrigo and van Dijken, 2011). Since then, however, sea ice has not shown the same degree of decline, and increases in NPP are due primarily to increased phytoplankton biomass, perhaps due to greater nutrient availability (Lewis et al., 2020). Spring blooms contribute substantially to annual Arctic primary production (Perrette et al., 2011), fuel upper trophic levels, and export carbon (Wassmann et al., 2004; Forest et al., 2011; Le Moigne et al., 2015). Overall, environmental changes in the Arctic Ocean have

[1] Department of Earth System Science, Stanford University, Stanford, CA, USA
[2] Cooperative Institute for Climate, Ocean, and Ecosystem Studies, University of Washington, Seattle, WA, USA
[3] School of Oceanography, University of Washington, Seattle, WA, USA
[4] Pacific Marine Environmental Laboratory, National Oceanic and Atmospheric Administration, Seattle, WA, USA
[5] Takuvik Joint International Laboratory, Laval University (Canada)–CNRS (France), Département de biologie et Québec-Océan, Université Laval, Québec City, QC, Canada
[6] Sorbonne Université and CNRS, Laboratoire d'Océanographie de Villefranche (LOV) UMR7093, Institut de la Mer de Villefranche (IMEV), Villefranche-sur-Mer, France

* Corresponding author:
Email: hjoyw@uw.edu

important impacts on primary production, with rippling effects through higher trophic levels.

Along with the environmental changes, phytoplankton bloom phenology and location have changed in recent years (Ardyna and Arrigo, 2020). Historically, phytoplankton were largely thought to bloom in the marginal ice zone (MIZ; Ardyna et al., 2020a), where melting sea ice allows for both increased light transmission into the surface ocean and stratification, concentrating phytoplankton in the well-lit and still nutrient-rich surface waters. There is now widespread evidence of phytoplankton blooming under sea ice (Ardyna et al., 2020a). This change is likely due to thinner sea ice with a more heterogeneous surface, allowing under-ice environments to receive enough light to support phytoplankton blooms (Ardyna et al., 2020a). In the future, phytoplankton blooms could shift towards greater development under sea ice than in the MIZ (Ardyna and Arrigo, 2020).

To thrive in an environment with continually changing light due to sea ice melt and movement, Arctic phytoplankton must balance investment in cellular machinery for light harvesting and carbon fixation (i.e., photosynthesis) with protection against excessive light (photoprotection) to avoid protein damage from light not used for photosynthesis (photodamage). Phytoplankton photoacclimate to their light environment in part by up-regulating photoprotective pigments (such as carotenoids and xanthophylls) in high light or up-regulating photosynthetic pigments (including chlorophylls) in low light (MacIntyre et al., 2000).

As phytoplankton mix throughout the water column, at times they are in near-surface waters where they are exposed to high light (relative to what they experience in the middle or bottom of the mixed layer) for periods of time on the order of minutes to hours. The differences between light that phytoplankton experience during mixing can be enhanced during sea ice retreat and can vary over two orders of magnitude (Lowry et al., 2018). The goal of our study was to investigate how phytoplankton respond to short periods (20 minutes) of greatly elevated light, similar to what under-ice phytoplankton would experience when the sea ice retreats or as phytoplankton are mixed throughout the water column. Our primary objective was to determine whether phytoplankton under the ice, in the MIZ, and in open water respond differently to short periods of high light exposure, and whether this exposure results in photophysiological changes. We conducted 21 FLuorescence After light SHock (FLASH) experiments in Baffin Bay to better understand how ephemeral changes in light influence phytoplankton photophysiology, including photoprotection and photodamage. Experiments were conducted on the Green Edge cruise (spring–summer 2016) that transited the sea ice edge, such that phytoplankton for experiments were sampled from under the ice, in the MIZ, and in open water to capture a progression of irradiance regimes.

2. Methods

2.1. Environmental conditions

2.1.1. Study region

Baffin Bay is ice-covered from December through May and, as ice melts in spring, the sea ice edge retreats westwards from Greenland towards Nunavut, Canada. To the north of our study area, waters in Baffin Bay circulate counterclockwise, driven by cold Arctic-derived waters entering northern Baffin Bay and transiting southwards along the coast of Nunavut (Platt et al., 1982). Warm and salty Atlantic-derived waters enter Baffin Bay through Davis Strait and transit northwards along the coast of Greenland. Eventually, water flows out of southwestern Baffin Bay (Melling et al., 2001; Bâcle et al., 2002). Consequently, Baffin Bay has an east–west gradient in water masses (Tremblay et al., 2002; Tang et al., 2004) that, along with sea ice, determines its hydrographic and ecological dynamics (Tremblay et al., 2006). Baffin Bay has a predictable spring phytoplankton bloom (Perrette et al., 2011; Randelhoff et al., 2019) that is typically dominated by diatoms, although *Phaeocystis pouchetti* is often present as well (Lovejoy et al., 2002; Degerlund and Eilertsen, 2010; Ardyna et al., 2020b).

Hydrographic and phytoplankton parameters were assessed at 32 "full" stations that included both hydrographic and biological sampling during the Green Edge cruise on the CCGS *Amundsen* in Baffin Bay from June 9 to July 10, 2016. FLASH experiments, used to assess photophysiology, were conducted at 19 full stations at subsurface depths. At two of the full stations, experiments were conducted at both surface and subsurface depths to target the subsurface chlorophyll *a* (chl *a*) maximum (SCM), for a total of 21 experiments. Stations where experiments were initiated were distributed among the seven longitudinal transects across the ice edge, spanning an area from 67°N to 71°N and 55°W to 64°W (**Figure 1**).

2.1.2. Sea ice cover

At each station, AMSR2 sea ice concentrations on a 3.125 km grid were used to determine the percent sea ice cover (Beitsch et al., 2014; Kaleschke and Tian-Kunze, 2016). We compared sea ice concentration on the day of sampling to the mean ice cover over the previous 3, 5, and 7 days, as well as the sea ice concentration on those days. None of these sea ice concentration metrics gave significantly different results, so we chose to use sea ice cover on our sampling day as our metric for sea ice cover. Stations were classified as ice-covered if there were >10 days until the station became ice-free, in the marginal ice zone (MIZ) if there were $\leq$10 days until the station became ice-free or if the station had been ice-free for $\leq$10 days, and in open water if the station had been ice-free for >10 days. Snow depth, ice thickness, and freeboard thickness were measured at stations where ice was present.

2.1.3. Hydrography

At each of the 32 full stations assessed in this study, a Sea-Bird SBE 911+ conductivity-temperature-depth (CTD) rosette system was used to collect water samples. Mixed layer depth (MLD) was determined from the maximum of Brunt-Väisälä buoyancy frequency (Carvalho et al., 2016), except at one station (St 318; **Table 1**) where a transient mixed layer was evident in the chl *a* concentration profile

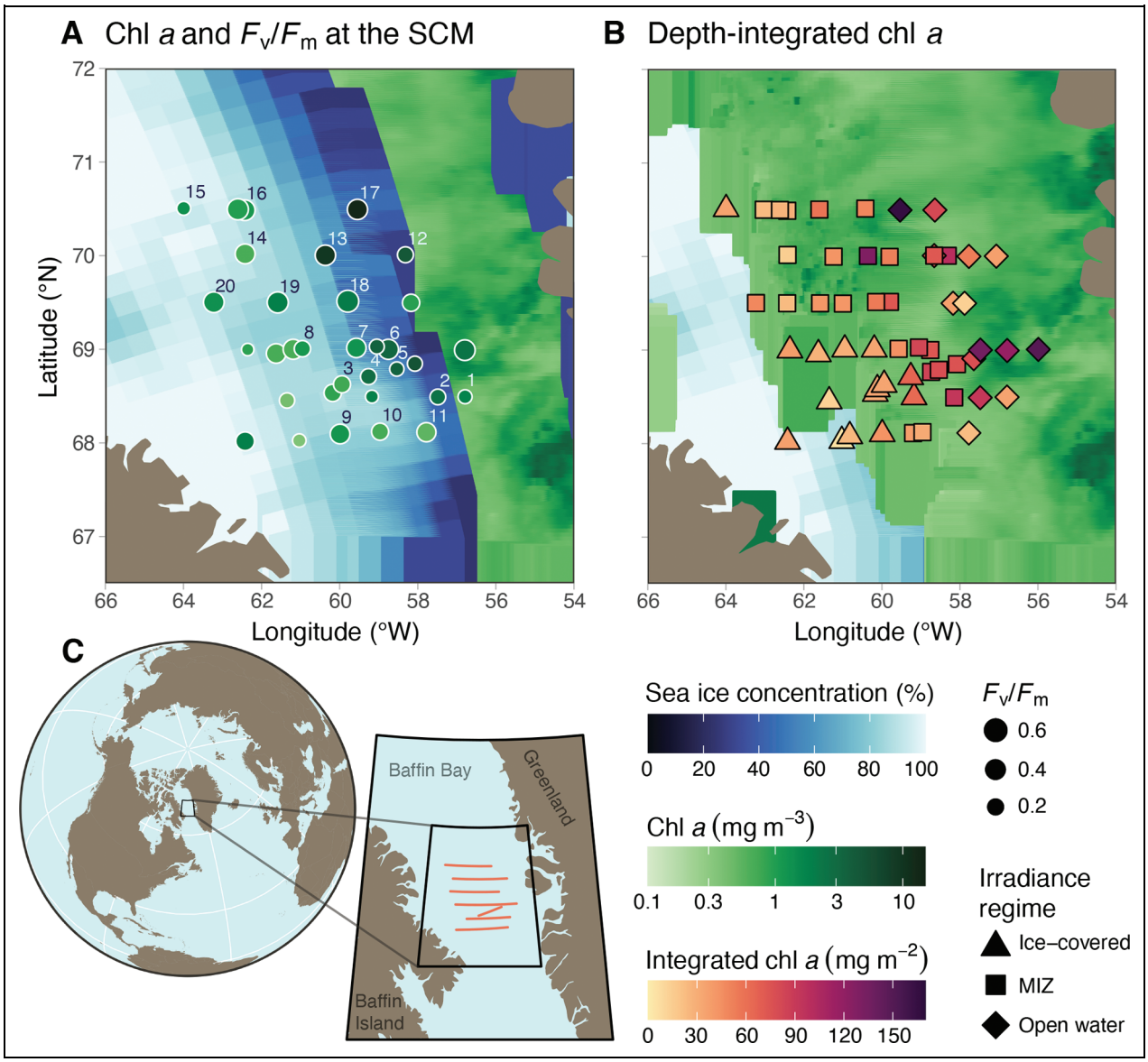

Figure 1. Map of study area. Study area shown with (A) in situ chlorophyll *a* (chl *a*) concentration and the ratio of variable fluorescence to maximum fluorescence (F_v/F_m) at the subsurface chl *a* maximum (SCM) and (B) depth-integrated chl *a* measured at each "full" station. Experiment locations are indicated with experiment numbers in (A); note that experiments were not conducted at every full station. In (A), color of points indicates chl *a* concentration (log scale) and size of points indicates F_v/F_m value. In (B), color of points indicates depth-integrated chl *a* and shape of points represents the irradiance regime: ice-covered (triangles), MIZ (squares), or open water (diamonds). Shown in the background of both panels are composite images of MODIS/Aqua satellite chl *a* concentration, level 3, 4 km resolution (green colorbar, same scale as in situ chl *a* concentration) during the cruise period (June 9 to July 10, 2016) and SSMIS satellite sea ice concentration (blue colorbar, where 0% ice concentration is not shown to allow chl *a* to be visible where there was no sea ice; https://nsidc.org/data/smmr_ssmi) on June 26, 2016 (mid-cruise). Areas where there was no sea ice are transparent; for areas where there was satellite data for both sea ice and chl *a*, panel (A) shows sea ice concentration and panel (B) shows chl *a* concentration. (C) Location of the study with cruise transects in orange. The black box represents the area shown in (A) and (B). Fewer stations are shown in (A) than in (B) because F_v/F_m was not measured at every station.

that the Brunt-Väisälä buoyancy frequency method did not identify. In this case, we assigned the MLD as the maximum depth before density crossed a threshold of $\Delta\sigma_\theta = 0.1$ kg m^{-3} (Peralta-Ferriz and Woodgate, 2015). Euphotic depth (E_z) was defined as the depth at which photosynthetically active radiation (PAR, 400–700 nm) was reduced to 1% of the incident PAR.

2.1.4. Dissolved nutrients

At each station where experiments were conducted, seawater samples from Niskin bottles on the CTD rosette were collected at 10 m intervals from 0 to 100 m, including the depth at which experiments were initiated. Samples were pre-filtered through 25 mm Whatman glass-fiber filters (GF/F, nominal pore size of 0.7 m) and

Table 1. Station location and hydrography where experiments were initiated, with photosynthetically active radiation (PAR) and nutrients at the depth sampled for experiments

Exp	Date (month-day in 2016)	Latitude (°N)	Longitude (°W)	Sampling Depth (m)	PAR (μmol photons m^{-2} s^{-1})	MLD[a] (m)	E_z (m)	Nitricline (m)	NO_3^- (μmol L^{-1})	PO_4^{3-} (μmol L^{-1})	$Si(OH)_4$ (μmol L^{-1})	Irradiance Regime
1	6-09	68.499	56.790	40	0.37	19.2	40.0	30	5.25	0.51	3.74	Open water
2	6-10	68.498	57.478	50	0.03	44.5	31.0	39	6.14	0.56	3.05	Open water
3	6-14	68.633	59.948	40	0.19	28.9	26.5	1	7.75	0.79	7.53	Ice-covered
4	6-15	68.708	59.256	15	1.40	10.5	21.5	7	2.10	0.32	2.32	Ice-covered
5	6-16	68.805	58.493	15	2.73	16.6	25.5	20	0.61	0.16	2.03	MIZ[b]
6	6-18	69.000	58.737	15	3.42	11.9	28.0	19	0.25	0.12	1.45	MIZ
7	6-19	69.012	59.562	15	0.44	14.1	15.4	0	3.36	0.47	4.46	MIZ
8	6-20	69.007	60.952	20	0.80	14.3	26.0	0	6.55	0.75	6.78	Ice-covered
9	6-26	68.107	59.995	20	0.79	10.7	27.0	0	4.85	0.59	5.20	Ice-covered
10	6-27	68.136	58.931	30	–[c]	2.0	–	7	5.13	0.52	4.23	MIZ
11	6-28	68.114	57.769	30	1.81	9.3	47.0	25	2.86	0.40	3.07	Open water
12	6-30	70.008	59.123	0	26.01	10.5	22.5	14	0.08	0.18	0.30	MIZ
12	6-30	70.008	59.123	10	3.66	10.5	22.5	14	0.59	0.26	0.63	MIZ
13	7-01	70.002	60.365	0	35.34	9.9	20.0	15	0.01	0.00	0.00	MIZ
14	7-01	70.002	60.365	15	2.00	9.9	20.0	15	0.08	0.29	1.44	MIZ
15	7-03	70.511	63.987	25	0.38	7.9	25.0	0	4.30	0.77	8.70	Ice-covered
16	7-04	70.504	62.518	20	3.05	17.2	41.0	0	3.25	0.55	6.71	MIZ
17	7-05	70.499	59.524	30	0.40	12.5	30.5	21	6.68	0.65	5.79	Open water
18	7-08	69.512	59.806	35	0.34	8.9	33.0	14	6.46	0.68	7.02	MIZ
19	7-09	69.501	61.582	20	1.16	10.3	35.0	15	4.66	0.66	6.73	MIZ
20	7-10	69.501	63.233	21	0.84	4.0	28.0	0	3.49	0.76	9.15	MIZ

[a]MLD: mixed layer depth.

[b]MIZ: marginal ice zone.

[c]Not available.

analyzed onboard for dissolved nutrients (NO_3^-, PO_4^{3-}, $Si(OH)_4$) on a Bran+Lebbe Autoanalyzer 3 using standard colorimetric methods (Grasshoff et al., 2009). The analytical detection limits were 0.03 μmol L^{-1} for NO_3^-, 0.05 μmol L^{-1} for PO_4^{3-}, and 0.1 μmol L^{-1} for $Si(OH)_4$.

Following Randelhoff et al. (2019), the nitracline depth was defined as the shallowest depth where NO_3^- concentration exceeded 1 μmol L^{-1}. NO_3^- concentration was linearly interpolated between vertical profile measurements spaced 10 m apart. Note that a nitracline depth of 0 m indicates that NO_3^- at that station was >1 μmol L^{-1} at all depths.

2.1.5. Irradiance

As described in Randelhoff et al. (2019), Compact Optical Profiling System (Biospherical Instruments, Inc.) multispectral irradiance profiles were measured to characterize underwater PAR profiles. Above-surface downwelling irradiance was measured synchronously as a reference to calculate the transmittance of PAR through sea ice down to the sea ice–seawater interface. To account for variable sea ice concentration, composite profiles were created for under sea ice and in open water from the closest measurements of transmittance under ice or in open water, respectively. Then, at each station, a percent transmission profile was calculated by weighting the ice-covered and open water profiles by the AMSR2-derived sea ice concentration. Finally, these transmission profiles were converted to vertical profiles of average daily PAR at each station by propagating the average daily PAR at the surface through the water column with the transmission profile at each station. PAR at the sampling depth at each station was then determined from this profile. To characterize the irradiance under sea ice at each station, we used the PAR at 3 m.

2.2. Phytoplankton abundance and physiology

2.2.1. Biomass

Pigments

Pigment samples were analyzed using high-performance liquid chromatography (HPLC) on an Agilent Technologies HPLC 1200 with a C8 guard column before the analytical column. One liter of sample was filtered on Whatman GF/F filters and stored in liquid nitrogen until analysis. For analysis, filters were extracted in 100% methanol for 2 hours, disrupted by sonication, clarified by filtration (GF/F Whatman, then 0.2 m PTFE), and measured using HPLC within 24 hours following Ras et al. (2008). For comparison, pigments were grouped into photosynthetic pigments (PSP = chl *a* + chl *b* + chl *c*1 + chl *c*2 + chl *c*3 + 19′-butanoyloxyfucoxanthin + 19′-hexanoyloxyfucoxanthin + fucoxanthin + peridinin + prasinoxanthin) and photoprotective pigments (PPP = diadinoxanthin (DD) + diatoxanthin (DT) + violaxanthin + zeaxanthin + lutein + carotenes). Both PSP and PPP were normalized to chl *a* concentration (Higgins et al., 2011; Van Leeuwe et al., 2014). There is some ambiguity as to whether 19′-butanoyloxyfucoxanthin plays more of a photoprotection or photosynthetic role in *Phaeocystis antarctica* (Van Leeuwe et al., 2014), but because our samples had low values of this pigment, the inclusion does not significantly alter our results.

The SCM was defined as the depth of maximum chl *a* concentration through the water column (10 depths from 0 to 100 m). This definition does not necessarily indicate that the waters above the SCM were devoid of nutrients or that they had extremely low chl *a* concentration. Depth-integrated chl *a* was calculated from the surface to 100 m, which was the deepest sampling depth, using trapezoidal integration.

Particulate organic carbon and nitrogen

Biomass was assessed by measuring particulate organic carbon (POC) and nitrogen (PON). Samples were collected by filtration under low vacuum pressure (< 5 mm Hg) onto precombusted (450°C for 4 hours) GF/F filters following Knap et al. (1996). This method does not remove inorganic carbon or nitrogen from the filters, so values for POC and PON may represent overestimates. Samples were dried (60°C for 24 hours) and stored at room temperature until post-cruise analysis on a Costech Elemental Analyzer using acetanilide as a calibration standard.

Phytoplankton community composition

As described in Ardyna et al. (2020b), the relative abundance of phytoplankton groups was determined using CHEMTAX software (Mackey et al., 1996). The CHEMTAX matrix was tuned for Arctic communities and a list of pigments used to identify taxa is available in Ardyna et al. (2020b). The groups clustered into the following chemotaxonomic classes: diatoms, dinoflagellates, cryptophytes, chryso-pelagophytes, prasinophytes (groups 2 and 3), chlorophytes, *Phaeocystis*, and haptophytes other than *Phaeocystis*. CHEMTAX-estimated community composition was closely related to Imaging FlowCytobot (IFCB) biovolume-estimated community composition (see methods in Massicotte et al., 2020), especially for diatoms, *Phaeocystis* (colonial form identified via IFCB), and other haptophytes. We therefore elected to use CHEMTAX-estimated community composition because we did not have IFCB samples for all stations and experiments.

Variable fluorescence

We measured the maximum photochemical efficiency of photosystem II (PSII; F_v/F_m) on a Pulse Amplitude Modulated fluorometer (Water-PAM, Heinz Walz). F_v/F_m is the ratio of variable fluorescence ($F_v = F_m - F_0$) to maximum fluorescence (F_m; Krause and Weis, 1991; Maxwell and Johnson, 2000). Prior to measurement, the Water-PAM was blanked with 0.2 m filtered seawater from the same station. Samples were dark-acclimated for 5 minutes before measurement to oxidize the photosynthetic reaction centers. However, our measurements represent a conservative estimate because there may have been some photons remaining downstream in the electron transport chain even following a dark acclimation period; thus, the dark-acclimated F_v/F_m may still be slightly suppressed relative to a completely unquenched F_v/F_m (Maxwell and Johnson, 2000).

2.2.2. Photosynthesis

Photosynthesis versus irradiance

Using methods described in Lewis and Smith (1983), photosynthesis versus irradiance (P-E) curves were used to determine maximum biomass-specific photosynthetic rates (P^*_{max}; mg C mg chl a^{-1} h^{-1}), light limited rates of photosynthesis (α^*; mg C mg^{-1} chl a h^{-1} (µmol photons m^{-2} s^{-1}) $^{-1}$), and the photoacclimation parameter (E_k; µmol photons m^{-2} s^{-1}). Briefly, 40 ml of seawater samples were spiked with 150–300 µl of radiolabelled bicarbonate ($H^{14}CO_3^-$). Next, 1.5 ml of sample was added to scintillation vials and incubated for 2 hours at 0°C under a gradient of 14 light levels, ranging from approximately 0 to 1000 µmol photons m^{-2} s^{-1} (cool white LEDs, LUXEON star by Phillips, 6500 K). The baseline ^{14}C was quantified by adding 50 µl of buffered formalin and acidifying triplicate samples. To quantify the total ^{14}C after spiking the sample, 20 µl of sample was added to 50 µl of ethanolomine and 5.5 ml of scintillation cocktail (Ecolume). After incubation, 50 µl of buffered formalin and 250 µl of 6 N hydrochloric acid was added and allowed to ventilate for 24 hours to drive off unincorporated inorganic carbon. Following ventilation, 5.5 ml of scintillation cocktail was added and vials were tightly capped, vortexed to mix, and run on a Packard liquid scintillation counter.

P^*_{max} was calculated as described in Arrigo et al. (2010) using a modified nonlinear least-squares regression relationship (Platt et al., 1980):

$$P^* = P^*_s\left(1 - e^{\frac{-\alpha^* E}{P^*_s}}\right)\left(e^{\frac{-\beta^* E}{P^*_s}}\right) \quad (1)$$

where P^* (mg C mg^{-1} chl a h^{-1}) is the chl a-specific photosynthetic rate at irradiance E (µmol photons m^{-2} s^{-1}), P^*_s (mg C mg^{-1} chl a h^{-1}) is the light-saturated photosynthetic rate without photoinhibition, and β^* is the photoinhibition term (mg C mg^{-1} chl a h^{-1} (µmol photons m^{-2} s^{-1}) $^{-1}$). P-E parameters were only used when the p-value of the curve fit was < 0.05. P^*_{max} was then calculated as:

$$P^*_{max} = P^*_s\left(\frac{\alpha^*}{\alpha^* + \beta^*}\right)\left(\frac{\beta^*}{\alpha^* + \beta^*}\right)^{\frac{\beta^*}{\alpha^*}}. \quad (2)$$

Finally, E_k was calculated as:

$$E_k = \frac{P^*_{max}}{\alpha^*}. \quad (3)$$

Light absorption

Particulate absorption (a_p) was measured by filtering samples (volumes varied from 0.2 to 2.7 L) onto a Milli-Q water-rinsed GF/F filter and measuring absorbance on a Perkin-Elmer Lambda-19 spectrophotometer in a 15 cm integrating sphere from 200 to 860 nm (1 nm steps), following methods in Bricaud et al. (2010). Optical densities were corrected for the pathlength amplification effect (Stramski et al., 2015) and converted into a_p coefficients. Absorption by non-algal particles (a_{nap}) was measured after extraction of the sample in methanol for at least 12 hours and optical densities were measured again on the de-pigmented and re-hydrated filter (Kishino et al., 1985). For both a_p and a_{nap} measurements, air was used as a reference beam (Stramski et al., 2015) for both samples and wet blank filters and stability of the spectrophotometer was confirmed before, during, and after each measurement series.

Absorption by phytoplankton ($a_{ph}(\lambda) = a_p(\lambda) - a_{nap}(\lambda)$, m^{-1}) normalized to HPLC-determined chl a gives the chl a-specific absorption coefficient for phytoplankton (a^*_{ph}, m^2 mg^{-1} chl a) at each wavelength of the P-E photosynthetron light source ($E(\lambda)$). The spectrally averaged chl a-specific absorption coefficient for phytoplankton ($\bar{a}^*$, m^2 mg^{-1} chl a) was then calculated as

$$\bar{a}^* = \frac{\sum_{400}^{700} a^*_{ph}(\lambda) \times E(\lambda)}{\sum_{400}^{700} E(\lambda)}. \quad (4)$$

Quantum yield of photosynthesis

The maximum quantum yield of photosynthesis (Φ_m, mol C mol^{-1} photons absorbed) was calculated as:

$$\Phi_m = \frac{\alpha^*}{43.2\bar{a}^*}. \quad (5)$$

2.2.3. FLASH experiments

We assessed the responses of phytoplankton to a simulated variable light environment using FLASH experiments (see **Table 1**). We initiated experiments at stations with ice concentrations ranging from 0 to 100% (Table S1) and with water from the chlorophyll maximum at each station. Phytoplankton samples were collected from the CTD in the mornings at the SCM for most experiments and just below the sea ice at 0 m for two experiments (**Table 1**). As described in Alderkamp et al. (2010; 2013) and Joy-Warren et al. (2019), we incubated phytoplankton in on-deck incubators with 20 minutes of in situ surface irradiance exposure (SIE; called the "light shock") followed by incubation at simulated in situ light levels (**Figure 2**).

Samples were incubated in PAR and ultraviolet radiation (UVR)-transparent Nasco Whirl-Pak bags (270–700 nm; UVC is not included because it is attenuated so strongly through the atmosphere that negligible amounts reach the surface of the ocean; Smith et al., 1992). The wavelength transmission through the Whirl-Pak bags was measured on a Perkin-Elmer Lambda 35 spectrophotometer by mounting pieces of the bags on the filter holder to allow light to pass directly through the filter.

The impacts of the light shock on phytoplankton fluorescence were measured over 2 hours following the light shock. Pigments, POC, P^*_{max}, α^*, E_k, $\bar{a}^*$, and Φ_m were measured 3.5 hours following the light shock (incubated at in situ light levels following 20-minute SIE) and compared to control samples that did not receive the light shock and were exclusively incubated at in situ light levels.

We evaluated the impact of initial environmental conditions and biological variables at each station where an

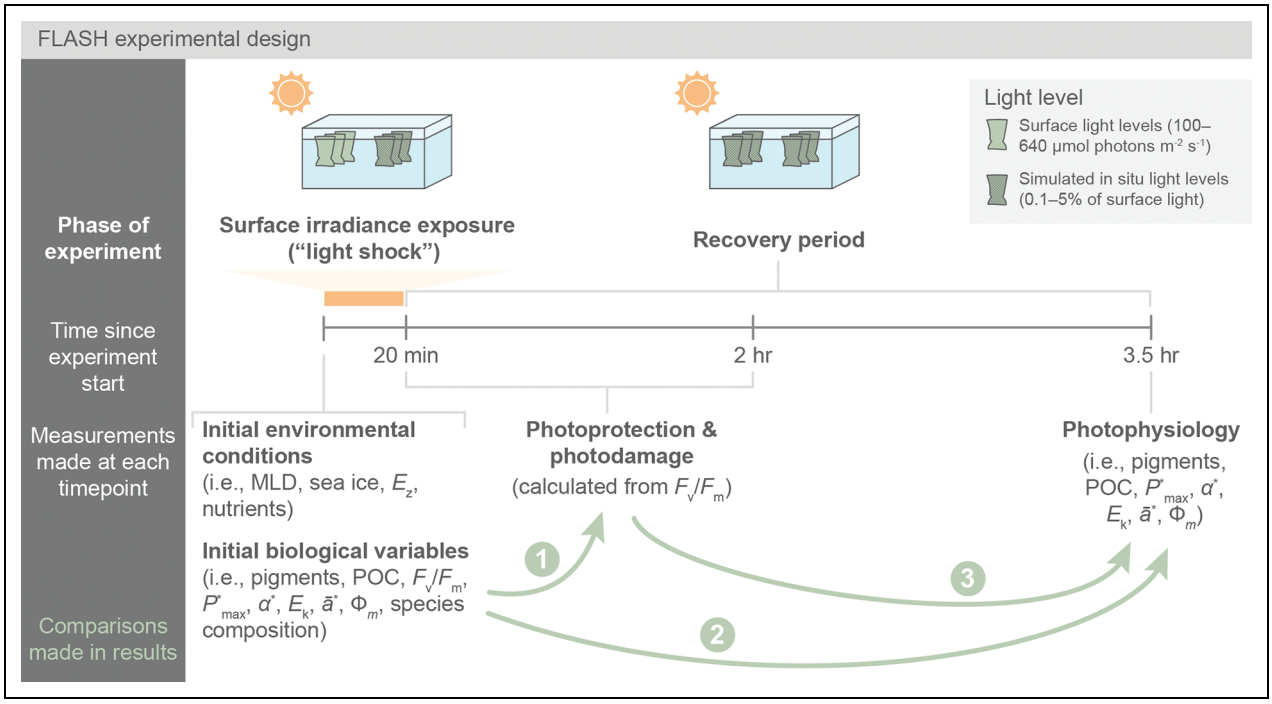

Figure 2. Design of FLuorescence After light SHock (FLASH) experiments. The two phases of the experiments (surface irradiance exposure and recovery at in situ light levels) are depicted with samples in whirlpak bags in triplicate within an incubator. In the timeline of the experiment, the light shock lasted 20 minutes, the resulting amount of photoprotection or photodamage was assessed during the first 2 hours of the recovery period using F_v/F_m measurements, and finally photophysiological parameters were measured 3.5 hours after the light shock. Light levels during the first 20 minutes were surface light levels (unshaded, light green Whirl-Pak bags) for the light-shock treatment and simulated in situ light levels (shaded, grey Whirl-Pak bags) for the controls (no light-shock treatment). All samples during the recovery period received simulated in situ light levels. Initial environmental conditions and biological variables were measured prior to the start of each experiment. Comparisons made in the Results section are shown with green arrows, and numbers indicate the order in which results are discussed.

experiment was initiated on the above parameters, as well as photoprotection and photodamage. These results are organized in three parts. First, we describe the impacts of initial environmental conditions on photoprotection and photodamage measured following the light shock (arrow 1 in **Figure 2**) and on the recovery of photosynthetic efficiency and pigments (quantified as the normalized difference between the light-shocked and control samples) measured 3.5 hours after the light shock (arrow 2 in **Figure 2**). Next, we describe the impacts of initial biological variables on the photoprotection, photodamage, photosynthetic efficiency, and pigments (arrows 1 and 2 in **Figure 2**). Finally, we describe the relationships among photophysiological parameters (photoprotection, photodamage, photosynthetic efficiency, and pigments; arrow 3 in **Figure 2**).

The sensitivity of phytoplankton to SIE was quantified as described in Joy-Warren et al. (2019), following Alderkamp et al. (2010; 2013). Briefly, F_0 and F_m were measured (see Methods: Variable fluorescence) before and immediately following the 20-minute SIE to record the initial impact of the light shock. Both F_0 and F_m were measured another three times at 40-minute intervals during a 2-hour recovery period at very low light (<1 µmol photons m^{-2} s^{-1}) and ambient seawater temperatures. This series of measurements during recovery allowed quantification of non-photochemical quenching of chl *a* fluorescence (*qN*) at each time point, calculated as follows:

$$qN = 1 - \frac{F_m' - F_0'}{F_m - F_0} \quad (6)$$

where F_m' is the maximum and F_0' is the minimum fluorescence following SIE relative to the maximum (F_m) and minimum (F_0) fluorescence before SIE (Van Kooten and Snel, 1990).

Under low and variable biomass, *qN* represents a more stable calculation of non-photochemical quenching than when it is calculated using the Stern-Volmer equation that gives the ratio of quenched to remaining fluorescence; thus we chose to calculate the former (Krause and Weis, 1991; Maxwell and Johnson, 2000; Lavaud et al., 2007; Alderkamp et al., 2013). Calculating *qN* over time allows for the quantification of the two relaxation components of *qN*: photoprotection (*qE*, fast-relaxing or energy-dependent quenching; xanthophyll cycling) and photodamage (*qI*, slow-relaxing quenching or photoinhibitory quenching; requires protein repair) (Maxwell and Johnson, 2000; Alderkamp et al., 2010; Alderkamp et al., 2013; Lavaud and Goss, 2014).

2.3. Statistical analysis

We present our statistical analysis in three parts. The first part uses all station data over the cruise to compare in situ phytoplankton communities among the three irradiance regimes (ice-covered, MIZ, and open water). The latter two parts test for possible relationships between either initial environmental conditions (part two) or biological parameters (part three) and photophysiology measured in the FLASH experiments.

Statistical analysis in Part 1

Over the cruise region, in situ environmental conditions and biological variables were grouped into three regimes based on time to/since sea ice retreat (see Methods: Sea ice cover). Because sea ice cover largely determines the amount of light that penetrates the surface of the ocean, each regime had distinct amounts of mean PAR in the mixed layer (see Results: Sea Ice and Hydrography); we took this classification to represent different irradiance regimes.

For each group, we took the mean of all measurements with sample depth $\leq$MLD to assess surface mixed layer samples only. However, results were consistent when we instead analyzed data from $\leq$10 m, $\leq$15 m, $\leq$20 m, $\leq$30 m, $\leq$40 m, and $\leq$SCM. We compared each variable among irradiance regimes using a 2-way analysis of variance (ANOVA; statistical software R). We analyzed significant ($p < 0.05$) ANOVA tests with the Tukey Honest Significant Difference test (Tukey HSD; statistical software R). Comparative words (higher/lower, more/less) are only used when differences are statistically significant at $p < 0.05$. The number of observations for each variable (n) in each irradiance regime is given in **Table 2** and ranged from 24 to 105.

Statistical analysis in Parts 2 and 3

We also analyzed photosynthetic parameters measured in the FLASH experiments grouped by irradiance regime (as for Part 1), although no experimental measurements showed significant differences among irradiance regimes, likely because of low sample size (21 experiments). We therefore treated our variables as continuous (as opposed to binned by ice cover) and analyzed the impacts of initial environmental conditions and biological parameters on the photophysiological parameters measured in the FLASH experiments with linear regressions (lm function; statistical software R; **Figure 2**).

The impact of the light shock on photosynthetic efficiency and pigments was assessed as the normalized difference between the light-shocked sample and control sample ((light-shocked sample − control)/control). Because the light shock was exposure to in situ light levels, there was a range of light-shock intensities. We present and discuss relationships when $p < 0.05$; comparative words are only used when a relationship is significant.

When a relationship is described as an initial condition positively correlated with the light-shock effect on a parameter, this correlation indicates that the larger the initial condition, the more the light shock increased the parameter relative to the control. The word "more" may refer to either a positive or a negative overall effect of the light shock, depending on whether samples fell above or below zero change from the light shock.

3. Results

3.1. Sea ice and nutrients

At the end of May 2016, our study site was almost entirely ice-covered, except for the stations furthest to the east (**Figure 1**). During the cruise, the ice retreated from east to west, initially retreating parallel with the coast of Greenland (until around June 23) and eventually retreating parallel to the coast of Nunavut. The study region was almost entirely ice-free by the end of our cruise (July 13). The cruise track was designed to transit across the MIZ, allowing us to sample the under-ice environment (40 stations; mean and standard deviation (SD) of 19 $\pm$ 5 days until ice retreat), the MIZ (60 stations; mean and SD of 1 $\pm$ 6 days since ice retreat), and the open water (35 stations; mean and SD of 20 $\pm$ 7 days since ice retreat; **Table 2**). These three regimes had distinct irradiance (PAR at 3 m): ice-covered had low light (66 $\pm$ 40 µmol photons m^{-2} s^{-1}), MIZ had moderate but variable light (202 $\pm$ 96 µmol photons m^{-2} s^{-1}), and open water had high light (267 $\pm$ 87 µmol photons m^{-2} s^{-1}). Photophysiological results are interpreted within the framework of the distinct irradiance in each of these regimes. For further description of sea ice during the Green Edge cruise, see Randelhoff et al. (2019).

Mean concentration of nutrients (NO_3^-, PO_4^{3-}, $Si(OH)_4$) in the mixed layer differed significantly among irradiance regimes. All three nutrients followed similar spatial patterns and were highest at ice-covered stations, partially depleted in the MIZ (NO_3^-: mean of 43% consumed relative to deep water >100 m), and low at open water stations (NO_3^-: mean of 54% consumed; see **Table 2**).

3.2. In situ phytoplankton communities

The mean POC concentration in the mixed layer was greater in the MIZ than in ice-covered waters, but neither region was different from the mean POC in open water (**Figure 3**). PON followed the same spatial pattern (**Table 2**). The highest mean chl *a* concentrations were observed in the MIZ and ice-covered waters, but only mean chl *a* concentration in the MIZ was greater than in open water (**Figure 1**). Depth-integrated chl *a*, however, was greater in open water than under the sea ice. The depth of the SCM differed by irradiance regime and was located near the surface in ice-covered waters (6 $\pm$ 6 m), deepening within the MIZ (18 $\pm$ 13 m) and reaching 37 $\pm$ 10 m in open water. The mean POC/chl *a* ratio was high in open water and lower in the MIZ and under sea ice.

Photoprotective pigments normalized to chl *a* concentration (PPP/ chl *a*) in the mixed layer were similar among the three irradiance regimes (mean and SD across cruise in the mixed layer: 0.19 $\pm$ 0.09). Photosynthetic pigment ratios (PSP/ chl *a*), on the other hand, were lower in higher irradiance environments, decreasing from 1.78 $\pm$ 0.11

Table 2. Mean ± standard deviation values (with *n* observations in parentheses) for station variables measured in the mixed layer of each irradiance regime, with Tukey HSD post-hoc significance level, where *p*: (no symbol) > 0.1 > ○ > 0.05 > ● > 0.01 > ●● > 0.001 > ●●● > 0

Station Variables[a]	Ice-Covered		MIZ[b]		Open Water		Ice-Covered vs. MIZ	Ice-Covered vs. Open Water	MIZ vs. Open Water
Open water days	−19 ± 5	(26)	1 ± 6	(39)	20 ± 7	(24)	●●●	●●●	●●●
Irradiance (PAR) at 3 m (μmol photons m^{-2} s^{-1})	66 ± 40	(26)	202 ± 96	(39)	267 ± 87	(24)	●●●	●●●	○
MLD (m)	15 ± 11	(26)	10 ± 7	(38)	22 ± 15	(24)		○	●●●
SCM (m)	6 ± 6	(26)	18 ± 13	(38)	37 ± 10	(24)	●●	●●●	●●●
NO_3^- (μmol L^{-1})	3.86 ± 1.45	(93)	1.24 ± 1.48	(100)	0.57 ± 1.5	(74)	●●●	●●●	●
PO_4^{3-} (μmol L^{-1})	0.66 ± 0.18	(91)	0.29 ± 0.22	(105)	0.15 ± 0.14	(89)	●●●	●●●	●●●
$Si(OH)_4$ (μmol L^{-1})	6.12 ± 1.89	(93)	2.85 ± 2.47	(102)	1.17 ± 1.14	(88)	●●●	●●●	●●●
POC (μg L^{-1})	193 ± 133	(45)	334 ± 177	(56)	278 ± 158	(41)	●		
PON (μg L^{-1})	32.0 ± 15.8	(45)	47.4 ± 18.7	(56)	39.1 ± 19.0	(41)	●		
Chl *a* (mg m^{-3})	0.92 ± 0.55	(70)	1.15 ± 0.92	(97)	0.62 ± 0.5	(61)			●●
Integrated chl *a* (mg m^{-2})	34 ± 16	(40)	59 ± 28	(60)	72 ± 46	(37)	○	●●	
F_v/F_m	0.25 ± 0.12	(68)	0.23 ± 0.12	(68)	0.23 ± 0.10	(40)			
POC/chl *a* (g:g)	182 ± 81	(44)	303 ± 179	(56)	940 ± 1073	(36)		●●	●●
(DD+DT)/chl *a*	0.09 ± 0.03	(70)	0.11 ± 0.07	(97)	0.11 ± 0.06	(61)			
PPP/chl *a*	0.16 ± 0.05	(70)	0.19 ± 0.09	(97)	0.20 ± 0.11	(61)			
PSP/chl *a*	1.78 ± 0.11	(70)	1.71 ± 0.09	(97)	1.65 ± 0.05	(61)	●●●	●●●	●●●
PPP/PSP	0.09 ± 0.03	(70)	0.11 ± 0.05	(97)	0.12 ± 0.06	(61)		●	
α^* (mg C mg^{-1} chl *a* h^{-1} (μmol photons m^{-2} s^{-1}) $^{-1}$)	0.076 ± 0.093	(55)	0.057 ± 0.074	(66)	0.094 ± 0.095	(36)			
P^*_{max} (mg C mg^{-1} chl *a* h^{-1})	2.98 ± 3.34	(55)	3.17 ± 4.69	(66)	4.60 ± 3.75	(36)			
E_k (μmol photons m^{-2} s^{-1})	48 ± 20	(55)	59 ± 25	(66)	76 ± 54	(36)		●	
$\bar{a}^*$ (m^2 mg^{-1} chl *a*)	0.018 ± 0.009	(53)	0.019 ± 0.004	(73)	0.022 ± 0.005	(38)			
Φ_m (mol C mol^{-1} photons absorbed)	0.095 ± 0.121	(53)	0.066 ± 0.084	(66)	0.119 ± 0.115	(35)			

[a]Definitions of station variables: PAR: photosynthetically active radiation; MLD: mixed layer depth; SCM: subsurface chlorophyll a maximum; NO_3^-: nitrate; PO_4^{3-}: phosphate; $Si(OH)_4$: silicate; POC: particulate organic carbon; PON: particulate organic nitrogen; Chl *a*: chlorophyll *a*; F_v/F_m: ratio of variable to maximum fluorescence; (DD+DT): diadinoxanthin + diatoxanthin; PPP: photoprotective pigments; PSP: photosynthetic pigments; α^*: light-limited rate of photosynthesis; P^*_{max}: maximum biomass-specific photosynthetic rate; E_k: photoacclimation parameter; $\bar{a}^*$: spectrally averaged chl *a*-specific absorption coefficient for phytoplankton; Φ_m: maximum quantum yield of photosynthesis.

[b]MIZ: marginal ice zone.

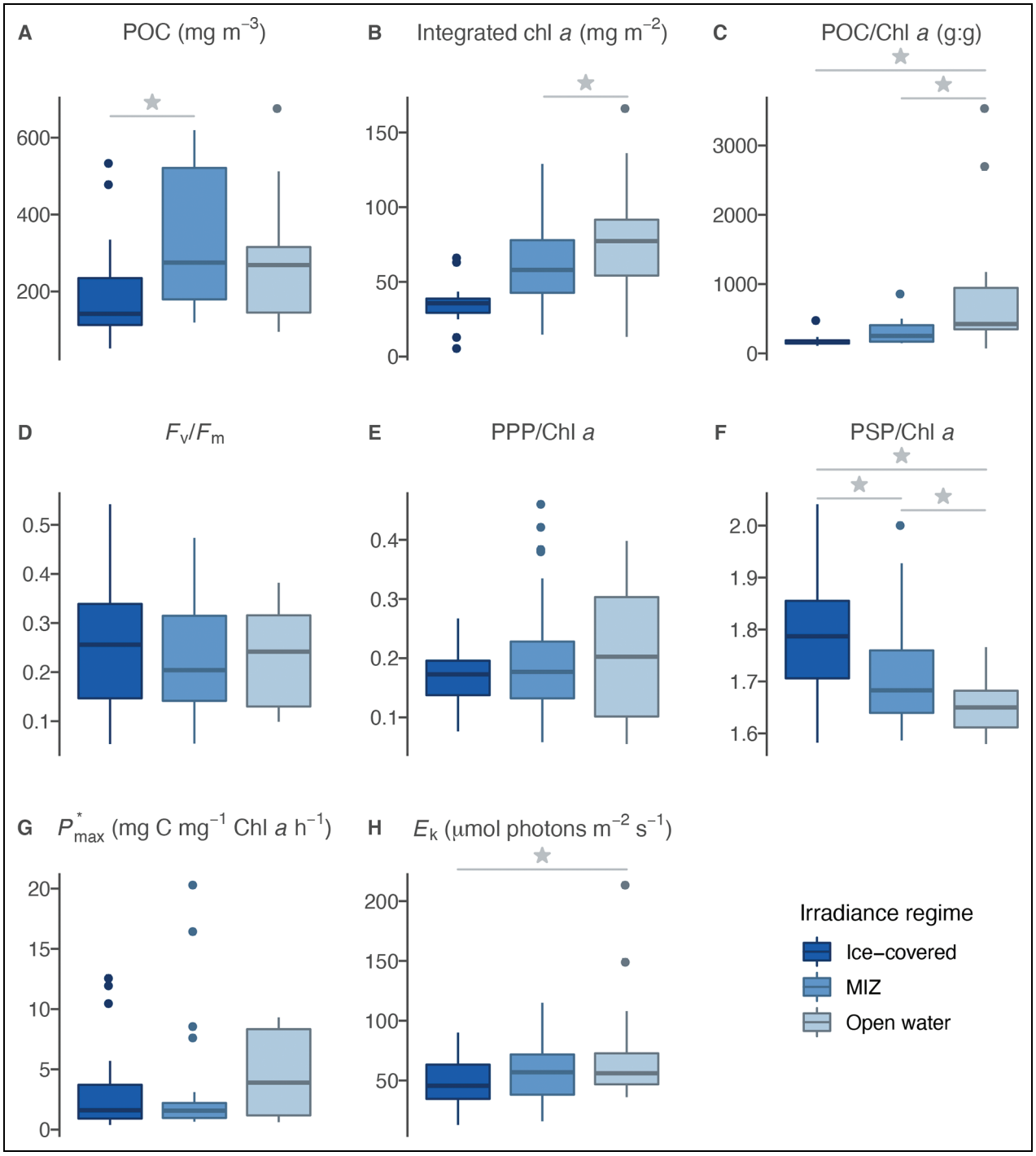

Figure 3. Biomass and physiology within the mixed layer of each irradiance regime. Box-and-whisker plots indicate, in horizontal lines from bottom to top, the 25%, 50% (median), and 75% quantiles. Vertical lines indicate ±1.5 × the interquartile range (or the maximum/minimum value if within the range). Points outside of this range are shown. Significant differences between regimes (connected by horizontal gray line) are shown with a star. When ice-covered and open water regimes are different, the connecting line extends over the marginal ice zone (MIZ) regime, but does not indicate that the MIZ is part of the comparison. POC: particulate organic carbon; chl *a*: chlorophyll *a*; F_v/F_m: ratio of variable to maximum fluorescence; PPP: photoprotective pigments; PSP: photosynthetic pigments; P^*_{max}: maximum biomass-specific photosynthetic rate; E_k: photoacclimation parameter.

under the ice to 1.65 ± 0.05 in open water (**Table 2**). There were no differences in (DD+DT)/chl *a* among irradiance regimes (**Table 2**), which ranged from 0.03 to 0.35 and averaged 0.10 ± 0.06. Although PPP/PSP displayed almost the same patterns as (DD+DT)/ chl *a*, PPP/PSP in open water was slightly higher than in ice-covered water.

The absorption coefficient ($\bar{a}^*$) was consistent among all three irradiance regimes, averaging 0.019 ± 0.006 m^2 mg^{-1} chl *a* and ranging from 0.004 to 0.046 m^2 mg^{-1} chl *a*. Mean F_v/F_m in the mixed layer was not different among irradiance regimes and averaged 0.24 ± 0.12 across the cruise, ranging from 0.05 to 0.54 (**Figure 1**).

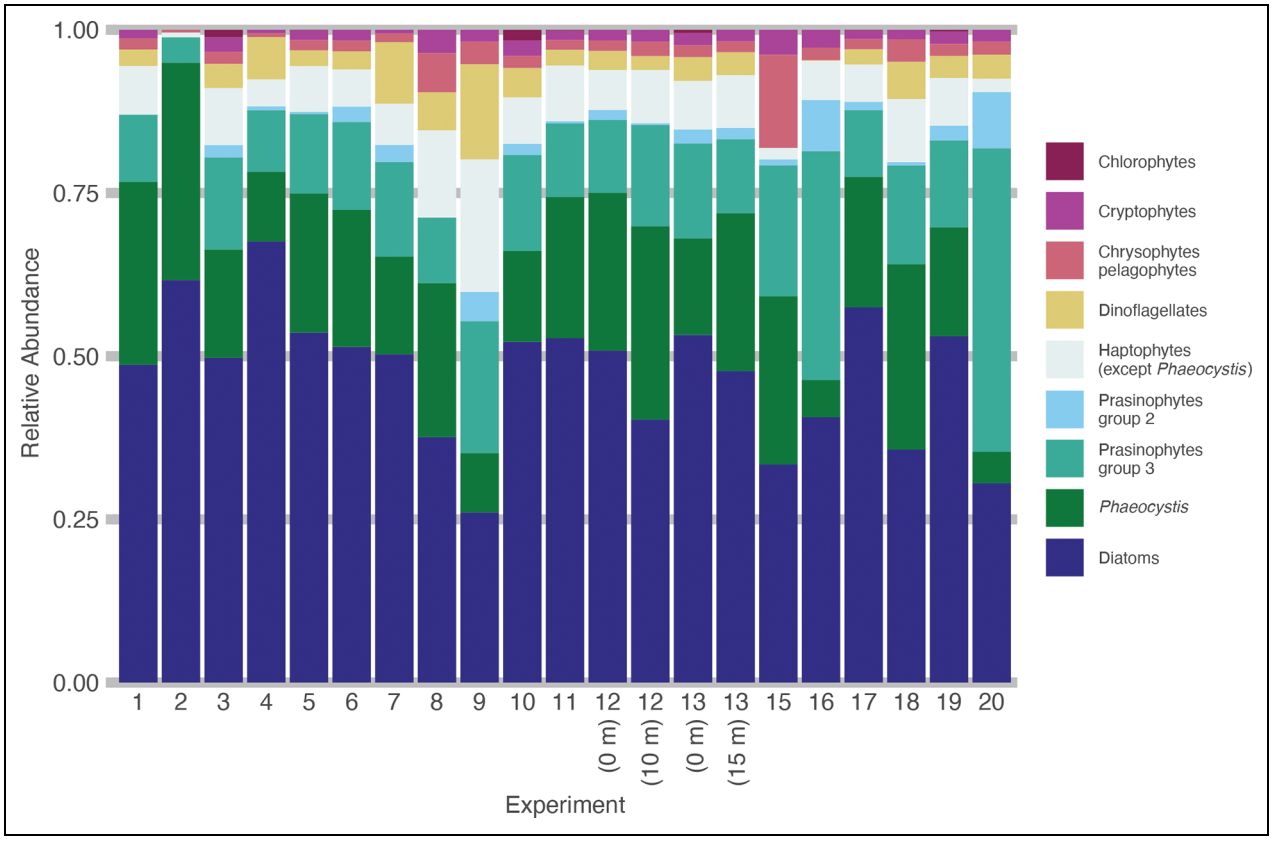

Figure 4. Initial phytoplankton community composition at depths sampled for experiments. Relative abundance of phytoplankton, color-coded by group, determined using CHEMTAX software. Where two depths were tested in the same experiment, depths are given to distinguish.

Of the carbon fixation parameters, only E_k differed among irradiance regimes. Despite high variability, mean E_k was higher in open water than under sea ice (**Table 2**). P^*_{max}, α^*, and Φ_m were highly variable during the cruise and none exhibited statistically significant differences among the three irradiance regimes. P^*_{max} ranged from 0.39 to 20.29 mg C mg^{-1} chl *a* h^{-1} and averaged 3.27 ± 3.96 mg C mg^{-1} chl *a* h^{-1}; α^* ranged from 0.004 to 0.363 mg C mg^{-1} chl *a* h^{-1} [µmol photons m^{-2} s^{-1}] $^{-1}$ and averaged 0.070 ± 0.085 mg C mg^{-1} chl *a* h^{-1} [µmol photons m^{-2} s^{-1}] $^{-1}$; and Φ_m averaged 0.085 ± 0.105 mol C mol^{-1} photons absorbed and ranged from 0.004 to 0.610 mol C mol^{-1} photons absorbed.

3.3. FLASH experiments

3.3.1. Phytoplankton community composition

Across our experiments, diatoms dominated the phytoplankton community (mean ± SD: 48 ± 12%; CHEMTAX relative pigment abundance), followed by *Phaeocystis* (20 ± 7%) and prasinophytes (group 3; 15 ± 9%). Dinoflagellates, cryptophytes, chryso-pelagophytes, prasinophytes (group 2), chlorophytes, and haptophytes (other than *Phaeocystis*) all made up less than 10% of the community on average, although at individual stations, one or more of these groups occasionally contributed up to 20% of the community (**Figure 4**).

Twelve experiments were diatom-dominated, with diatoms making up between 25 and 49% of the community in the other nine experiments (**Figure 4**). At the stations for which we have IFCB biovolume-estimated community composition (Experiments 13, 15, 17, 18, 19, and 20), there was high variability in the composition of the diatom community. Although on average centric (55 ± 44%) and pennate (44 ± 42%) diatoms each made up approximately half of the community, at individual stations the range for each was from ≤5% to ≥94%. IFCB images revealed that the diatom community was made up of the genera *Attheya*, *Chaetoceros*, *Coscinodiscales*, *Cylindrotheca*, *Entomoneis*, *Eucampia*, *Melosira*, *Nitzschia* (*N. frigida*), *Porosira*, *Synedropsis*, and *Thalassiosira*, as well as unidentified pennate and centric diatoms. *Thalassiosira* (55 ± 38%) made up the bulk of the diatom community by biovolume, followed by unidentified pennate (40 ± 39%) and centric (22 ± 30%) diatoms, and *Melosira* (12 ± 10%). The remaining groups made up an average of <10% of the diatom community by biovolume, except in Experiment 13 (0 m) where *Porosira* made up 42% and in Experiment 15 where *Synedropsis* made up 15% of the diatom community. For a description of the diatom community across the entire cruise, see Lafond et al. (2019).

Some studies have shown that photophysiological changes are influenced by community composition (Moore et al., 2006; Suggett et al., 2009). However, initial community composition in our experiments was fairly uniform and our results compare differences in treatments over 3.5 hours, over which time we would not expect significant changes in community composition. We therefore consider

Table 3. Non-photochemical quenching, photoprotection, and photodamage measured in each experiment, with photosynthetically active radiation (PAR) at the sampling depth and during the light shock, as well as the ratio between the two PAR values

Exp	PAR at Sampling Depth (μmol photons m^{-2} s^{-1})	PAR during Light Shock (μmol photons m^{-2} s^{-1})	Light-Shock PAR/PAR at Sampling Depth	Non-Photo-Chemical Quenching	Photo-Protection	Photo-Damage
1	4.11	181 ± 57	44	0.64	0.00	1.00
2	0.03	640 ± 6	22,201	0.83	0.51	0.33
3	0.19	194 ± 74	1046	0.88	0.20	0.71
4	1.40	309 ± 17	221	0.88	0.21	0.70
5	2.73	357 ± 64	131	1.03	0.25	0.75
6	3.42	622 ± 101	182	0.98	0.08	0.97
7	0.44	333 ± 39	753	0.98	0.00	1.00
8	0.80	565 ± 59	709	0.93	0.05	0.90
9	0.79	246 ± 19	310	0.98	0.03	0.98
11	1.81	284 ± 20	156	0.99	0.00	0.98
12 (0 m)	26.01	277 ± 11	11	1.04	0.10	0.94
12 (10 m)	3.66	270 ± 12	74	1.01	0.00	1.00
13 (0 m)	35.34	525 ± 45	15	0.77	0.13	0.82
13 (15 m)	2.00	481 ± 77	240	0.97	0.05	0.95
15	0.38	391 ± 54	1023	1.01	0.01	0.98
17	0.40	300 ± 26	750	1.01	0.00	1.00
18	0.34	188 ± 9	555	0.95	0.03	0.92
19	1.16	104 ± 13	89	0.89	0.18	0.70
20	0.84	276 ± 13	328	1.02	0.02	1.00

our results indicative of treatment effects rather than effects of differing community composition.

3.3.2. Photophysiology as a function of environmental conditions

Photoprotection and photodamage

Non-photochemical quenching was negatively correlated with photoprotection ($p = 0.013$) and positively correlated with photodamage ($p = 0.002$), suggesting that the higher the non-photochemical quenching, the less photoprotection and the more photodamage resulted from the light shock (**Table 3**).

Both the MLD and nitracline were positively correlated with photoprotection (MLD: $p < 0.001$; nitracline: $p = 0.021$) and negatively correlated with photodamage (MLD: $p < 0.001$; nitracline: $p = 0.038$; **Figure 5**). Sea ice concentration and thickness, freeboard thickness, days to open water, E_z, PAR at sampling depth, and nutrients (NO_3^-, PO_4^{3-}, $Si(OH)_4$) were not significantly related to non-photochemical quenching, photoprotection, or photodamage.

Photosynthetic efficiency and pigments

MLD was positively correlated with the light-shock effect on P^*_{max} ($p = 0.033$) and Φ_m ($p = 0.003$), meaning that phytoplankton from stations with a deeper mixed layer exhibited a greater reduction in P^*_{max} due to the light shock. E_z was negatively correlated with the light-shock effect on (DD+DT)/chl *a* ($p = 0.006$), indicating that the light shock had a more positive effect when E_z was shallow. PPP/PSP was negatively correlated ($p = 0.009$) and Φ_m was positively correlated ($p = 0.043$) with mean PAR during the light shock, while α^* was positively correlated ($p = 0.004$) and F_v/F_m was negatively correlated ($p = 0.044$) with the ratio of light received during the 3.5-hour incubation to PAR at sampling depth. The thickness of the ice freeboard was positively correlated with both (DD+DT)/chl *a* ($p = 0.025$) and PPP/PSP ($p = 0.031$). The number of days until the station became ice-free after sampling was negatively correlated with the effect of the light shock on (DD+DT)/chl *a* ($p = 0.049$). The effect of the light shock on F_v/F_m was negatively correlated with NO_3^- ($p = 0.04$) and PO_4^{3-} ($p = 0.009$) at the sampling depth.

3.3.3. Photophysiology as a function of biological variables

Photoprotection and photodamage

Initial concentrations of chl *a*, POC, and PON, as well as the ratios POC/chl *a*, (DD+DT)/chl *a*, and PPP/PSP, did not

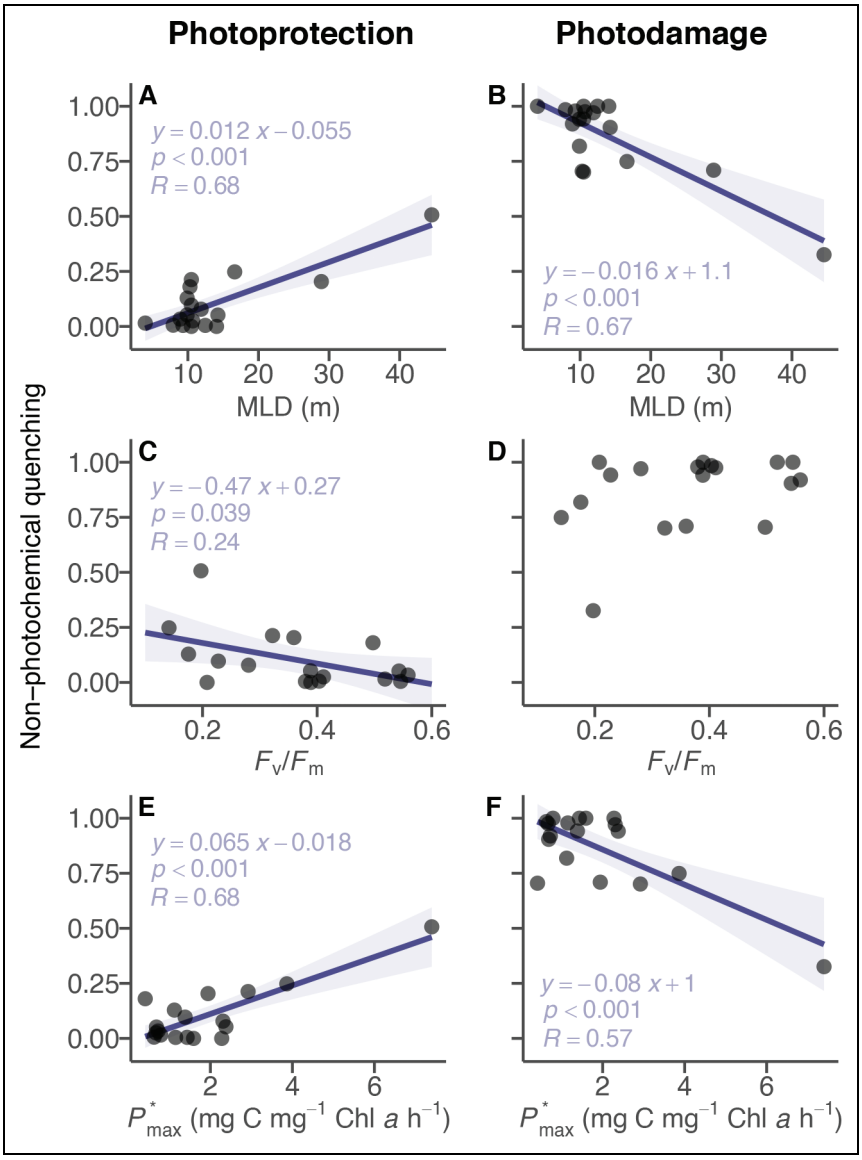

Figure 5. Relationships between initial variables and non-photochemical quenching (separated into photoprotection and photodamage) in FLuorescence After light SHock (FLASH) experiments. Left panels (A, C, E) show relationships for photoprotection; right panels (B, D, F), for photodamage. Initial variables, measured at the station and depth sampled for each experiment, are the mixed layer depth (MLD; A, B), maximum photochemical efficiency of PSII reaction centers (F_v/F_m; C, D), and maximum biomass-specific photosynthetic rate (P^*_{max}; E, F). Solid lines indicate linear regressions, with statistics noted in each panel; shaded areas indicate 95% confidence limits.

influence non-photochemical quenching, photoprotection, or photodamage. Photoprotection was greatest in samples with low F_v/F_m ($p = 0.039$; **Figure 5**). High initial P^*_{max}, α^*, and Φ_m resulted in greater photoprotection (P^*_{max}:$p < 0.001$; α^*: $p = 0.001$; Φ_m: $p < 0.001$) and lower photodamage (P^*_{max}: $p < 0.001$; α^*: $p = 0.002$; Φ_m: $p = 0.001$). Initial β^* was not correlated with non-photochemical quenching, photoprotection, or photodamage.

Samples with a high proportion of diatoms exhibited a high degree of photoprotection ($p = 0.014$), while samples with a low diatom proportion exhibited high photodamage ($p = 0.019$). The initial fraction of dinoflagellates, chryso-pelagophytes, cryptophytes, chlorophytes, prasinophytes, *Phaeocystis*, and other haptophytes were not correlated with non-photochemical quenching, photoprotection, or photodamage.

Photosynthetic efficiency and pigments

Initial F_v/F_m was negatively correlated with the light shock-effect on F_v/F_m ($p = 0.038$). Initial P^*_{max} was positively correlated with the light-shock effect on PON ($p = 0.010$), while initial β^* was positively correlated with the light-shock effects on α^* ($p = 0.034$) and β^* ($p = 0.038$). Initial $\bar{a}^*$ was negatively correlated with POC/chl *a* ($p = 0.016$) and P^*_{max} ($p = 0.011$). Initial chl *a* concentration, (DD+DT)/chl *a*, PPP/PSP, and Φ_m were not correlated with effects of the light shock.

Haptophyte abundance (other than *Phaeocystis*) was positively correlated with the magnitude of the light

shock-effect on both α^* ($p = 0.08$) and $\bar{a}^*$ ($p = 0.048$), while chlorophyte abundance was positively correlated with the magnitude of the light-shock effect on β^* ($p < 0.001$). The effect of the light shock on chl *a* concentration was positively correlated with, and POC/chl *a* was negatively correlated with, initial cryptophyte (chl *a*: $p = 0.027$; POC/chl *a* $p = 0.014$) and chryso-pelagophyte abundance (chl *a*: $p < 0.001$; POC/chl *a* $p < 0.001$). Chryso-pelagophytes were also negatively correlated with the light-shock effect on P^*_{max} ($p = 0.033$) and $\bar{a}^*$ ($p = 0.037$). Initial chlorophyte abundance ($p < 0.001$) was positively correlated with the light-shock effect on F_v/F_m . Diatom abundance was not correlated with photophysiological effects of the light shock.

3.3.4. Relationships among photophysiological parameters

The effect of the light shock on F_v/F_m was negatively correlated with non-photochemical quenching ($p = 0.03$) and positively correlated with photoprotection ($p = 0.03$). The effect of the light shock on Φ_m was positively correlated with photoprotection ($p = 0.021$) and negatively correlated with photodamage ($p = 0.015$).

The effects of the light shock on (DD+DT)/chl *a* and PPP/PSP were positively correlated with each other ($p < 0.001$), and PPP/PSP was positively correlated with POC/chl *a* ($p = 0.048$). The effect of the light shock on chl *a* concentration was negatively correlated with POC/chl *a* ($p < 0.001$), P^*_{max} ($p = 0.005$), and $\bar{a}^*$ ($p < 0.001$).

The effect of the light shock on P^*_{max} was positively correlated with the effects on POC/chl *a* ($p = 0.025$), α^* ($p = 0.042$), and Φ_m ($p = 0.029$). Additionally, the effect on α^* was positively correlated with Φ_m ($p < 0.001$). The effect on $\bar{a}^*$ was positively correlated with the effect on POC/chl *a* ($p = 0.001$), while both α^* ($p = 0.001$) and Φ_m ($p = 0.002$) were negatively correlated with the effect on E_k .

4. Discussion

4.1. Key environmental factors drive seasonal phytoplankton dynamics

The Green Edge cruise sampled three different irradiance regimes, which were characterized by distinct hydrographic patterns. The MLD was shallowest in the MIZ where ice melt stratifies the water column, and deepest in open water where wind energy can reach the surface of the ocean and deepen surface mixing (**Table 2**; Randelhoff et al., 2019). Nutrients in the mixed layer followed a predictable pattern with ice concentration: elevated under ice and increasingly depleted with decreasing ice cover (**Table 2**). The SCM also followed the expected pattern of deepening with reduced ice concentrations, a commonly observed phenomenon where phytoplankton concentrate at the depth of the optimal combination of light (highest at surface) and nutrients (highest at depth; Martin et al., 2010; Ardyna et al., 2011). As phytoplankton in surface waters deplete surface nutrients, the community must concentrate deeper and deeper to access nutrients (Tremblay et al., 2008). With the seasonal transition from spring to summer, increasing solar irradiance and ice melt result in deeper light penetration through the water column that can support phytoplankton growth at depth.

4.2. In situ biomass and photosynthetic pigments differed among irradiance regimes

Concentrations of POC, PON, and chl *a* were within range of previous observations in Baffin Bay (Harrison and Platt, 1986; Harrison et al., 1987). Mean POC (**Figure 3**) and chl *a* concentration displayed the opposite pattern among irradiance regimes (**Table 2**). As a result, the cellular POC/chl *a* ratio demonstrated large differences among irradiance regimes. POC/chl *a* was lowest in the ice-covered regime (mean ± SD: 182 ± 81 g:g; lowest irradiance) and highest in open water (940 ± 1073 g:g; highest irradiance). Detritus and zooplankton are likely contributing to the POC in our samples, making the POC/chl *a* ratios especially high.

The POC/chl *a* ratios in the ice-covered (182 ± 81 g:g) and MIZ (303 ± 179 g:g) regimes reflect those commonly seen across seasons in the Arctic. For example, Lewis et al. (2018, a three-year study from spring to summer in the Chukchi Sea) observed POC/chl *a* of 119 ± 120 g:g in the early season "low-light, high-nutrient" (sea ice cover > 80%; NO_3^- > 3 μmol L^{-1}) period, which increased to 314 ± 170 g:g by the late season "high-light, low-nutrient" (sea ice cover < 10%; NO_3^- < 1 μmol L^{-1}) period. In the Chukchi and Beaufort seas, Palmer et al. (2013) measured POC/chl *a* of 50 ± 83 to 91 ± 83 g:g under the ice and 67 ± 83 to 143 ± 125 g:g in open water. Under pack ice north of Svalbard, however, Assmy et al. (2017) measured POC/chl *a* ratios much lower (31.4 g:g) than those measured even under sea ice in this study.

The ratio of photosynthetic pigments to chl *a* (PSP/chl *a*) also differed among irradiance regimes (**Figure 3**). Under the ice, where light was low but nutrients required for biosynthesis were replete (**Table 2**), phytoplankton produced large amounts of photosynthetic pigments to optimize their light acquisition (Geider et al., 1993; Geider et al., 1998). In the higher light regimes (MIZ and open water) phytoplankton reduced their internal concentrations of photosynthetic pigments (including chl *a*; **Table 2**), as they were no longer needed (Mac-Intyre et al., 2002; Kropuenske et al., 2009; Nymark et al., 2009; Arrigo et al., 2010). Correspondingly, the photoacclimation parameter (E_k) was higher in open water than under sea ice (**Table 2**), demonstrating that phytoplankton cells had photoacclimated to the increase in light from the under-ice to the open water regime.

4.3. In situ carbon fixation was similar among irradiance regimes

P^*_{max} was high in all three regimes (means of 3.0–4.6 mg C mg^{-1} chl *a* h^{-1}), despite much lower NO_3^- in the open water regime than in the other regimes (**Table 2**). Our measurements were within range, but on average higher, than those previously reported in summer in Baffin Bay (Harrison and Platt, 1986). For comparison, Lewis et al. (2018) reported a mean P^*_{max} value of 2.42 ± 0.92 mg C mg^{-1} chl *a* h^{-1} in low-light, high-nutrient waters (comparable to our ice-covered regime) and 0.83 ± 0.45 mg C

mg^{-1} chl *a* h^{-1} in high-light, low-nutrient waters (comparable to our open water regime). In the Beaufort Sea, Palmer et al. (2011) measured P^*_{max} values with means of 0.93 ± 0.54 mg C mg^{-1} chl *a* h^{-1} under the ice and 0.71 ± 0.38 mg C mg^{-1} chl *a* h^{-1} in open water. Notably, in our study P^*_{max} was consistently high and variable across regimes, while Palmer et al. (2011) similarly observed little difference between ice-covered and open water regions, but lower P^*_{max} overall, and Lewis et al. (2018) observed a lower P^*_{max} in high-light, low-nutrient waters than in low-light, high-nutrient waters. NO_3^- concentrations in our study region closely mirrored those measured in the Chukchi Sea by Lewis et al. (2018): mean values of NO_3^- were 3.86 ± 1.45 µmol L^{-1} in our ice-covered regime and 0.57 ± 1.5 µmol L^{-1} in open water. Thus, despite low light under the ice and low NO_3^- in open water, P^*_{max} did not appear to be light- or nutrient-limited overall, the latter of which Harrison et al. (1982) and Harrison and Platt (1986) also observed in Baffin Bay in the summer. However, given the high variability in P^*_{max}, there was likely patchy light- or nutrient-limitation in each regime. Overall our photosynthetic rates were far less light- and/or nutrient-limited than those observed by either Palmer et al. (2011) or Lewis et al. (2018) and indicate that despite some possible limitations, photosynthesis was generally not limited in the late spring in Baffin Bay.

4.4. In situ phytoplankton have similar photoprotective states under ice cover and in open water

Despite distinct hydrographic, biomass, and pigment patterns, the photoprotective status of the phytoplankton communities in each irradiance regime was very similar, mirroring the photosynthetic parameters. Phytoplankton generally synthesize more photoprotective pigments as a strategy to acclimate to high light (Brunet et al., 2011). Photoprotective pigments within the mixed layer (including the xanthophyll cycle pigments, DD+DT) did not differ among irradiance regimes, but were in fact quite high across all three regimes (study-wise mean PPP/chl *a*: 0.19 ± 0.09; study-wise mean (DD+DT)/chl *a*: 0.10 ± 0.06). For comparison, also in Baffin Bay, Alou-Font et al. (2016) found PPP/chl *a* ratios that averaged 0.14 ± 0.06 at ice-covered stations, similar to a combination of our under-ice and MIZ regimes, and 0.24 ± 0.05 at open-water stations, about twice as much light as our open water regime. The same pattern in (DD+DT)/chl *a* holds between the two studies. Lewis et al. (2018) found mean PPP/chl *a* ratios between 0.074 ± 0.017 (early season) and 0.153 ± 0.065 (late season) in the Chukchi Sea. These values suggest that, in this study, phytoplankton growing under the ice in Baffin Bay already had sufficient photoprotective mechanisms in place for a rapid transition to higher light. This same phenomenon, described as phytoplankton "priming" for rapid growth once light increases, was demonstrated by Lewis et al. (2018) in the Chukchi Sea.

F_v/F_m, the photochemical efficiency of PSII reaction centers, did not change among the irradiance regimes and was fairly low (mean: 0.24 ± 0.12). The consistency in F_v/F_m across irradiance regimes may support the suggestion that phytoplankton are primed for future high light (Lewis et al., 2018). However, F_v/F_m also displayed a high amount of variability (range: 0.05 to 0.54). Given the potential for small-scale variability when ice cover is heterogeneous (Ardyna et al., 2020a), this high variability may indicate that phytoplankton are locally acclimated, with photophysiological states that vary widely within an irradiance regime. Considering that we did not observe differences in photoprotective pigments or F_v/F_m among irradiance regimes, however, we conclude that phytoplankton in all three regimes were similarly photoacclimated.

4.5. Few environmental conditions impacted the extent of photoprotection or photodamage

As with the in situ measurements (see sections 4.2, 4.3, and 4.4), ice conditions and light had little impact on how phytoplankton responded to the light shock in our FLASH experiments (data not shown), supporting our conclusion that phytoplankton are largely prepared for high light even when originating in under-ice, low-light environments. Photoprotection was higher and photodamage was lower when samples came from deeper mixed layers (**Figure 5**), where phytoplankton also exhibited high P^*_{max}, α^*, and Φ_m and low F_v/F_m. When phytoplankton came from stations with deep mixed layers, they were better able to protect themselves and were less photodamaged. Conversely, when phytoplankton came from stations with shallow mixed layers they were less able to protect themselves and experienced greater photodamage. MLDs were very shallow (13.5 ± 9.0 m) at the stations where experiments were initiated and, as a result, most of the samples used for experiments came from depths below the mixed layer (experiments were initiated with water from the SCM). Thus, we expect that phytoplankton sampled at stations where samples were collected from within the mixed layer were in fact exposed to higher in situ light (and therefore more photophysiologically prepared for the light shock) than samples from stations where mixed layers were much shallower than the sampling depth, thereby preventing exposure to surface irradiance. This expectation would be the case in both an average sense (mean mixed layer light is higher than below the mixed layer) and an episodic sense (intermittent mixing toward the surface).

Photoprotection was greatest in samples with low initial F_v/F_m and high initial P^*_{max}, α^*, and Φ_m. When cells were optimized to make use of low light (high α^*), had a high quantum yield of photosynthesis (Φ_m), and achieved high maximum rates of photosynthesis (high P^*_{max}), they were able to protect themselves from high light. Surprisingly, cells with low F_v/F_m also demonstrated a high degree of photoprotection (**Figure 5**), potentially because the photons that would have been measured as variable fluorescence (F_v) were instead dissipated through photoprotective mechanisms, reducing the measured F_v/F_m (MacIntyre et al., 2000). Alternatively, cells that initially had a high proportion of damaged photosystems (low F_v/F_m) may have been forced to photoprotect against excess light because they did not have sufficient functioning

photosystems to make use of the elevated light (MacIntyre et al., 2000).

Surprisingly, neither sea ice concentration nor the intensity of PAR at the depth from which FLASH experiments were initiated influenced the degree of photoprotection or photodamage. Additionally, neither initial (DD+DT)/chl *a* nor PPP/PSP were correlated with photoprotection or photodamage, nor were initial chl *a*, POC, and PON concentrations, or initial POC/chl *a*. These experimental results may either indicate that phytoplankton are photophysiologically similar under varying ice and light conditions in Baffin Bay, enabling quick responses to rapid changes in light (Lewis et al., 2018), or reflect the capacity of diatoms to cope with large fluctuations in light (Lavaud et al., 2007).

4.6. Photoprotection and photodamage were temporary

Phytoplankton were generally able to recover photophysiologically from the light shock within 3.5 hours, as evidenced by the similarity of most parameters before and after the light shock, with the exception of F_v/F_m and Φ_m. Interestingly, the effects of the light shock on F_v/F_m and Φ_m were not correlated. In experiments where phytoplankton exhibited a high degree of photoprotection, the light shock increased F_v/F_m relative to the control, indicating that when cells were protecting themselves from excess light, they were also able to repair damaged photosystems (Bouchard et al., 2005a; Bouchard et al., 2005b; Alderkamp et al., 2010). F_v/F_m likely increased because cells were repairing the D1 protein, part of the PSII reaction center complex (Aro et al., 1993; Falkowski and Raven, 2007). Despite the high metabolic expense of repairing the D1 protein, it is essential to repair the photosystems that shuttle photons from photosynthetic pigments to the remainder of the photosynthetic electron transport chain, a process that can happen on the order of 30 minutes (Ohad et al., 1984; Ohad et al., 1990). Thus, elevated F_v/F_m when cells are photoprotecting indicates cellular investment in protein repair that will enable elevated rates of photosynthesis.

P^*_{max}, α^*, E_k, PPP/PSP, (DD+DT)/chl *a*, and $\bar{a}^*$ were unaffected by the light shock after 3.5 hours of recovery. Photosynthetic rate has been shown to recover following UV radiation exposure in approximately 2–6 hours, depending on phytoplankton community assemblage and kinetic repair rate (Boucher and Prézelin, 1996; Fritz et al., 2008). Photoprotective pigments, in particular DD and DT, likely responded to the light shock rapidly (within 1 hour) with reversible transformations of a fraction of the DD pool into DT, but with no new pigment synthesis (Demers et al., 1991). After 3.5 hours, then, the only pigment changes that likely took place were within the xanthophyll cycle pigment pool (DD and DT). However, the initial photoacclimation state of the phytoplankton allowed cells to accommodate rapid changes in light. The light shock influenced the overall light environment to which cells acclimated through a longer-term build up of photoprotective mechanisms (Sakshaug et al., 1987; Demers et al., 1991).

5. Conclusion

Both our in situ measurements and our FLASH experiments demonstrate that phytoplankton under the ice, in the MIZ, and in open water in Baffin Bay had differences in their biomass and pigments, yet similar photosynthetic and photoprotective states. We observed high concentrations of photoprotective pigments in phytoplankton in all three irradiance regimes, as well as high P^*_{max} in phytoplankton beneath sea ice and very high P^*_{max} in open water phytoplankton. These findings lend evidence to the idea that Arctic phytoplankton under the sea ice are primed to bloom once they have access to sufficient light (Lewis et al., 2018).

Despite observing photodamage in our experiments, we saw almost complete recovery from the light shock after 3.5 hours. Additionally, phytoplankton originating from all irradiance regimes responded photophysiologically similarly to the light shock. This further indicates that early season phytoplankton in the Arctic are acclimated to higher light than they are experiencing and are prepared for rapid changes in light.

These findings are important to consider as the Arctic continues to change rapidly, particularly in the context of sea ice cover. To understand the impact of sea ice changes on phytoplankton biomass and populations, we need to understand the photophysiology of Arctic phytoplankton. In our study, we show that at the time of year when snow on sea ice has mostly melted, nothing is preventing a bloom from starting under sea ice. This is demonstrated by, among other things, the lack of strong differences in E_k among the different regimes. In our study, phytoplankton were able to cope with variations in light over multiple orders of magnitude, suggesting that Arctic phytoplankton are capable of thriving in a changing Arctic light-scape. As sea ice thins and retreats earlier in the season, phytoplankton will be exposed to elevated irradiance earlier in the growing season (Kahru et al., 2011; Katlein et al., 2015; Katlein et al., 2019); under ice blooms are also expected to increase in prevalence (Ardyna et al., 2020a). Our work has demonstrated that, photophysiologically, phytoplankton are prepared to bloom under sea ice, likely contributing to changing biomass and species distributions. Future work investigating other Arctic regions, variability within irradiance regimes compared to variability among regimes, and species-specific variability in response to changing light will elucidate how Arctic phytoplankton will respond to environmental changes.

Data accessibility statement

Data used in this paper can be found here: https://www.seanoe.org/data/00487/59892/. Other data associated with the Green Edge project can be found here: http://www.obs-vlfr.fr/proof/php/GREENEDGE/greenedge.php. FLuorescence After light SHock (FLASH) experimental data can be found here: DOI: https://dx.doi.org/10.25740/jj290fk1806. IFCB taxonomy data can be found here: https://ecotaxa.obs-vlfr.fr/prj/144.

Supplemental files

The supplemental files for this article can be found as follows:

Table S1. Station data, including bottom depth, temperature, salinity, and snow and ice conditions, when experiments were initiated.

Acknowledgments

We would like to thank the Green Edge science team, especially Flavienne Bruyant for coordinating the cruise logistics, as well as the officers and crew members on the CCGC *Amundsen*. We would also like to thank Céline Dimier and Joséphine Ras for HPLC measurements, Annick Bricaud and Antoine Sciandra for absorption measurements, Achim Randelhoff for providing physical datasets, Nicole Garcia for nutrient analyses, Patrick Raimbault for POC and PON measurements, Pierre-Luc Grondin for identifying IFCB images, and Tonya Burgers for providing DIC data (Miller et al., 2020).

Funding

The GreenEdge project is funded by the following French and Canadian programs and agencies: ANR (Contract #111112), ArcticNet, CERC on Remote sensing of Canada's new Arctic frontier, CNES (project #131425), French Arctic Initiative, Fondation Total, CSA, LEFE and IPEV (project #1164). This project was conducted using the Canadian research icebreaker CCGS *Amundsen* with the support of the Amundsen Science program funded by the Canada Foundation for Innovation (CFI) Major Science Initiatives (MSI) Fund. The project was conducted under the scientific coordination of the Canada Excellence Research Chair on Remote sensing of Canada's new Arctic frontier and the CNRS & Université Laval Takuvik Joint International Laboratory (UMI3376). This research was also sponsored by the NSF Office of Polar Programs (PLR-1304563) to KRA.

Competing interests

Kevin Arrigo, a co-author, is also an associate editor for *Elementa*.

Author contributions

- Substantial contributions to conception and design: HJW, KRA, MB.[AQ1]
- Acquisition of data: HJW, KML, JET.
- Analysis and interpretation of data: HJW, KRA, MA.
- Drafting the article or revising it critically for important intellectual content: HJW, KRA, MA, MB, JET, KML.
- Final approval of the version to be published: HJW, KRA, MA, MB, JET, KML.

References

Alderkamp, AC, **de Baar, H**, **Visser, R**, **Arrigo, K.** 2010. Can photoinhibition control phytoplankton abundance in deeply mixed water columns of the Southern Ocean? *Limnology and Oceanography* **55**(3): 1248–1264. DOI: https://dx.doi.org/10.4319/lo.2010.55.3.1248.

Alderkamp, AC, **Mills, M**, **van Dijken, G**, **Arrigo, K.** 2013. Photoacclimation and non-photochemical quenching under in situ irradiance in natural phytoplankton assemblages from the Amundsen Sea, Antarctica. *Marine Ecology Progress Series* **475**: 15–34. DOI: https://dx.doi.org/10.3354/meps10097.

Alou-Font, E, **Roy, S**, **Agust, S**, **Gosselin, M.** 2016. Cell viability, pigments and photosynthetic performance of Arctic phytoplankton in contrasting ice-covered and open-water conditions during the spring–summer transition. *Marine Ecology Progress Series* **543**: 89–106. DOI: https://dx.doi.org/10.3354/meps11562.

Arctic Monitoring and Assessment Programme. 2017. Snow, Water, Ice and Permafrost in the Arctic (SWIPA). Available at http://www.amap.no/documents/doc/Snow-Water-Ice-and-Permafrost-in-the-Arctic-SWIPA-2017/1610.[AQ2]

Ardyna, M, **Arrigo, KR**. 2020. Phytoplankton dynamics in a changing Arctic Ocean. *Nature Climate Change* **10**: 1–12. DOI: https://dx.doi.org/10.1038/s41558-020-0905-y.

Ardyna, M, **Babin, M**, **Gosselin, M**, **Devred, E**, **Rainville, L**, **Tremblay, JÉ.** 2014. Recent Arctic Ocean sea ice loss triggers novel fall phytoplankton blooms. *Geophysical Research Letters* **41**(17): 6207–6212. DOI: https://dx.doi.org/10.1002/2014GL061047.

Ardyna, M, **Gosselin, M**, **Michel, C**, **Poulin, M**, **Tremblay, JÉ.** 2011. Environmental forcing of phytoplankton community structure and function in the Canadian High Arctic: Contrasting oligotrophic and eutrophic regions. *Marine Ecology Progress Series* **442**: 37–57. DOI: https://dx.doi.org/10.3354/meps09378.

Ardyna, M, **Mundy, C**, **Mayot, N**, **Matthes, LC**, **Oziel, L**, **Horvat, C**, **Leu, E**, **Assmy, P**, **Hill, V**, **Matrai, PA**, **Gale, M**, **Melnikov, IA**, **Arrigo, KR**. 2020a. Under-ice phytoplankton blooms: Shedding light on the "invisible" part of Arctic primary production. *Frontiers in Marine Science* **7**: 985. DOI: https://dx.doi.org/10.3389/fmars.2020.608032.

Ardyna, M, **Mundy, C**, **Mills, MM**, **Oziel, L**, **Grondin, PL**, **Lacour, L**, **Verin, G**, **van Dijken, G**, **Ras, J**, **Alou-Font, E**, **Babin, M**, **Gosselin, M**, **Tremblay, J-É**, **Raimbault, P**, **Assmy, P**, **Nicolaus, M**, **Claustre, H**, **Arrigo, KA**. 2020b. Environmental drivers of under-ice phytoplankton bloom dynamics in the Arctic Ocean. *Elementa: Science of the Anthropocene* **8**(1). DOI: https://dx.doi.org/10.1525/elementa.430.

Aro, EM, **McCaffery, S**, **Anderson, JM.** 1993. Photoinhibition and D1 protein degradation in peas acclimated to different growth irradiances. *Plant Physiology* **103**(3): 835–843. DOI: https://dx.doi.org/10.1104/pp.103.3.835.

Arrigo, K, **Mills, M**, **Kropuenske, L**, **van Dijken, G**, **Alderkamp, AC**, **Robinson, D.** 2010.

Photophysiology in two major Southern Ocean phytoplankton taxa: Photosynthesis and growth of *Phaeocystis antarctica and Fragilariopsis cylindrus* under different irradiance levels. *Integrative and Comparative Biology* **50**(6): 950–966. DOI: https://dx.doi.org/10.1093/icb/icq021.

Arrigo, KR, **van Dijken, G**, **Pabi, S.** 2008. Impact of a shrinking Arctic ice cover on marine primary production. *Geophysical Research Letters* **35**(19). DOI: https://dx.doi.org/10.1029/2008GL035028.

Arrigo, KR, **van Dijken, GL.** 2011. Secular trends in Arctic Ocean net primary production. *Journal of Geophysical Research: Oceans* **116**(C9). DOI: https://dx.doi.org/10.1029/2011JC007151.

Assmy, P, **Fernández-Méndez, M**, **Duarte, P**, **Meyer, A**, **Randelhoff, A**, **Mundy, CJ**, **Olsen, LM**, **Kauko, HM**, **Bailey, A**, **Chierici, M.** 2017. Leads in Arctic pack ice enable early phytoplankton blooms below snow-covered sea ice. *Scientific Reports* **7**: 1–9. DOI: https://dx.doi.org/10.1038/srep40850.

Bâcle, J, **Carmack, EC**, **Ingram, RG.** 2002. Water column structure and circulation under the North Water during spring transition: April–July 1998. *Deep Sea Research Part II: Topical Studies in Oceanography* **49**(22–23): 4907–4925. DOI: https://dx.doi.org/10.1016/S0967-0645(02)00170-4.

Beitsch, A, **Kaleschke, L**, **Kern, S.** 2014. Investigating high-resolution AMSR2 sea ice concentrations during the February 2013 fracture event in the Beaufort Sea. *Remote Sensing* **6**(5): 3841–3856. DOI: https://dx.doi.org/10.3390/rs6053841.

Bouchard, JN, **Campbell, DA**, **Roy, S**. 2005a. Effects of UV-B radiation on the D1 protein repair cycle of natural phytoplankton communities from three latitudes (Canada, Brazil, and Argentina). *Journal of Phycology* **41**(2): 273–286. DOI: https://dx.doi.org/10.1111/j.1529-8817.2005.04126.x.

Bouchard, JN, **Roy, S**, **Ferreyra, G**, **Campbell, DA**, **Curtosi, A**. 2005b. Ultraviolet-B effects on photosystem II efficiency of natural phytoplankton communities from Antarctica. *Polar Biology* **28**(8): 607–618. DOI: https://dx.doi.org/10.1007/s00300-005-0727-4.

Boucher, NP, **Prézelin, BB.** 1996. An *in situ* biological weighting function for UV inhibition of phytoplankton carbon fixation in the Southern Ocean. *Marine Ecology Progress Series* **144**: 223–236. DOI: https://dx.doi.org/10.3354/meps144223.

Bricaud, A, **Babin, M**, **Claustre, H**, **Ras, J**, **Tièche, F.** 2010. Light absorption properties and absorption budget of Southeast Pacific waters. *Journal of Geophysical Research: Oceans* **115**(C8). DOI: https://dx.doi.org/10.1029/2009JC005517.

Brunet, C, **Johnsen, G**, **Lavaud, J**, **Roy, S.** 2011. Pigments and photoacclimation processes, in Roy, S, LLewellyn, CA, Egeland, ES, Johnsen, G eds., *Phytoplankton pigments—Characterization, chemotaxonomy and applications in oceanography*, *1st ed.* Cambridge, UK: Cambridge University Press: 445–471. Available at https://hal.archives-ouvertes.fr/hal-01101814.

Carvalho, F, **Kohut, J**, **Oliver, M**, **Sherrell, R**, **Schofield, O.** 2016. Mixing and phytoplankton dynamics in a submarine canyon in the West Antarctic Peninsula. *Journal of Geophysical Research: Oceans* **121**: 5069–5083. DOI: https://dx.doi.org/10.1002/2016JC011650.

Comiso, JC, **Parkinson, CL**, **Gersten, R**, **Stock, L.** 2008. Accelerated decline in the Arctic sea ice cover. *Geophysical Research Letters* **35**(1). DOI: https://dx.doi.org/10.1029/2007GL031972.

Degerlund, M, **Eilertsen, HC.** 2010. Main species characteristics of phytoplankton spring blooms in NE Atlantic and Arctic waters (68–80 N). *Estuaries and Coasts* **33**(2): 242–269. DOI: https://dx.doi.org/10.1007/s12237-009-9167-7.

Demers, S, **Roy, S**, **Gagnon, R**, **Vignault, C.** 1991. Rapid light-induced changes in cell fluorescence and in xanthophyll-cycle pigments of *Alexandrium excavatum* (Dinophyceae) *and Thalassiosira pseudonana* (Bacillariophyceae): A photo-protection mechanism. *Marine Ecology Progress Series* **76**(2): 185–193. Available at https://www.jstor.org/stable/24825562.

Falkowski, P, **Raven, J**. 2007. *Aquatic photosynthesis. 2nd ed.* Princeton, NJ: Princeton University Press. DOI: https://dx.doi.org/10.1515/9781400849727.

Forest, A, **Tremblay, JÉ**, **Gratton, Y**, **Martin, J**, **Gagnon, J**, **Darnis, G**, **Sampei, M**, **Fortier, L**, **Ardyna, M**, **Gosselin, M**, **Hattori, H**, **Nguyen, D**, **Maranger, R**, **Vaqué, D**, **Marrasé, C**, **Pedrós-Alió, C**, **Sallon, A**, **Michel, C**, **Kellogg, C**, **Deming, J**, **Piepenburg, D**. 2011. Biogenic carbon flows through the planktonic food web of the Amundsen Gulf (Arctic Ocean): A synthesis of field measurements and inverse modeling analyses. *Progress in Oceanography* **91**(4): 410–436. DOI: https://dx.doi.org/10.1016/j.pocean.2011.05.002.

Fritz, JJ, **Neale, PJ**, **Davis, RF**, **Peloquin, JA.** 2008. Response of Antarctic phytoplankton to solar UVR exposure: Inhibition and recovery of photosynthesis in coastal and pelagic assemblages. *Marine Ecology Progress Series* **365**: 1–16. DOI: https://dx.doi.org/10.3354/meps07610.

Geider, RJ, **La Roche, J**, **Greene, RM**, **Olaizola, M.** 1993. Response of the photosynthetic apparatus of *Phaeodactylum tricornutum* (Bacillariophyceae) to nitrate, phosphate, or iron starvation. *Journal of Phycology* **29**(6): 755–766. DOI: https://dx.doi.org/10.1111/j.0022-3646.1993.00755.x.

Geider, RJ, **MacIntyre, HL**, **Kana, TM.** 1998. A dynamic regulatory model of phytoplanktonic acclimation to light, nutrients, and temperature. *Limnology and Oceanography* **43**(4): 679–694. DOI: https://dx.doi.org/10.4319/lo.1998.43.4.0679.

Grasshoff, K, **Kremling, K**, **Ehrhardt, M.** 2009. *Methods of seawater analysis. Third, completely revised and extended edition*. Weinheim, Germany: Verlag Chemie GmbH.

Harrison, W, **Li, W**, **Smith, J**, **Head, E**, **Longhurst, A.** 1987. Depth profiles of plankton, particulate organic matter and microbial activity in the Eastern

Canadian Arctic during summer. *Polar Biology* **7**(4): 207–224. DOI: https://dx.doi.org/10.1007/BF00287417.

Harrison, W, **Platt, T.** 1986. Photosynthesis–irradiance relationships in polar and temperate phytoplankton populations. *Polar Biology* **5**(3): 153–164. DOI: https://dx.doi.org/10.1007/BF00441695.

Harrison, W, **Platt, T**, **Irwin, B.** 1982. Primary production and nutrient assimilation by natural phytoplankton populations of the Eastern Canadian Arctic. *Canadian Journal of Fisheries and Aquatic Sciences* **39**(2): 335–345. DOI: https://dx.doi.org/10.1139/f82-046.

Higgins, H, **Wright, S**, **Schlüter, L.** 2011. Quantitative interpretation of chemotaxonomic pigment data, in Roy, S, Llewellyn, C, Egeland, E, Johnsen, G eds., *Phytoplankton pigments: Characterization, chemotaxonomy and applications in oceanography*. Cambridge, UK: Cambridge University Press: 257–313. DOI: https://dx.doi.org/10.1017/cbo9780511732263.010.

Intergovernmental Panel on Climate Change. 2019. Intergovernmental Panel on Climate Change Special Report on the Ocean and Cryosphere in a Changing Climate. Available at https://www.ipcc.ch/srocc/.[AQ3]

Joy-Warren, HL, **van Dijken, GL**, **Alderkamp, AC**, **Leventer, A**, **Lewis, KM**, **Selz, V**, **Lowry, KE**, **van de Poll, W**, **Arrigo, KR.** 2019. Light is the primary driver of early season phytoplankton production along the western Antarctic Peninsula. *Journal of Geophysical Research: Oceans* **124**: 1–25. DOI: https://dx.doi.org/10.1029/2019JC015295.

Kahru, M, **Brotas, V**, **Manzano-Sarabia, M**, **Mitchell, B.** 2011. Are phytoplankton blooms occurring earlier in the Arctic? *Global Change Biology* **17**(4): 1733–1739. DOI: https://dx.doi.org/10.1111/j.1365-2486.2010.02312.x.

Kaleschke, L, **Tian-Kunze, X.** 2016. *AMSR2 ASI 3.125 km Sea Ice Concentration Data, V0.1*. Institute of Oceanography, University of Hamburg, Germany.

Katlein, C, **Arndt, S**, **Belter, HJ**, **Castellani, G**, **Nicolaus, M.** 2019. Seasonal evolution of light transmission distributions through Arctic sea ice. *Journal of Geophysical Research: Oceans* **124**(8): 5418–5435. DOI: https://dx.doi.org/10.1029/2018JC014833.

Katlein, C, **Arndt, S**, **Nicolaus, M**, **Perovich, DK**, **Jakuba, MV**, **Suman, S**, **Elliott, S**, **Whitcomb, LL**, **McFarland, CJ**, **Gerdes, R**, **Boetius, A**, **German, CR**. 2015. Influence of ice thickness and surface properties on light transmission through Arctic sea ice. *Journal of Geophysical Research: Oceans* **120**(9): 5932–5944. DOI: https://dx.doi.org/10.1002/2015JC010914.

Kishino, M, **Takahashi, M**, **Okami, N**, **Ichimura, S.** 1985. Estimation of the spectral absorption coefficients of phytoplankton in the sea. *Bulletin of Marine Science* **37**(2): 634–642.

Knap, A, **Michaels, A**, **Close, A**, **Ducklow, H**, **Dickson, A**, eds. 1996. *Protocols for the Joint Global Ocean Flux Study (JGOFS) Core Measurements, JGOFS Report Nr. 19*, vol. vi+170 pp., (JGOFS Report Nr. 19, vol. vi+170 pp.). Reprint of the IOC Manuals and Guides No. 29, UNESCO 1994.

Krause, G, **Weis, E**. 1991. Chlorophyll fluorescence and photosynthesis: The basics. *Annual Review of Plant Physiology and Plant.* DOI: https://dx.doi.org/10.1146/annurev.pp.42.060191.001525.

Kropuenske, L, **Mills, M**, **van Dijken, G**, **Bailey, S**, **Robinson, D**, **Welschmeyer, N**, **Arrigo, K.** 2009. Photophysiology in two major Southern Ocean phytoplankton taxa: Photoprotection in *Phaeocystis antarctica* and *Fragilariopsis cylindrus*. *Limnology and Oceanography* **54**(4): 1176–1196. DOI: https://dx.doi.org/10.4319/lo.2009.54.4.1176.

Kwok, R. 2018. Arctic sea ice thickness, volume, and multiyear ice coverage: Losses and coupled variability (1958–2018). *Environmental Research Letters* **13**(10): 105005. DOI: https://dx.doi.org/10.1088/1748-9326/aae3ec.

Kwok, R, **Rothrock, D.** 2009. Decline in Arctic sea ice thickness from submarine and ICESat records: 1958–2008. *Geophysical Research Letters* **36**(15). DOI: https://dx.doi.org/10.1029/2009GL039035.

Lafond, A, **Leblanc, K**, **Quéguiner, B**, **Moriceau, B**, **Leynaert, A**, **Cornet, V**, **Legras, J**, **Ras, J**, **Parenteau, M**, **Garcia, N**, **Babin, M**, **Tremblay, J-É**. 2019. Late spring bloom development of pelagic diatoms in Baffin Bay. *Elementa: Science of the Anthropocene* **7**(44). DOI: https://dx.doi.org/10.1525/elementa.382.

Lavaud, J, **Goss, R.** 2014. The peculiar features of non-photochemical fluorescence quenching in diatoms and brown algae, in *Non-Photochemical Quenching and Energy Dissipation in Plants, Algae and Cyanobacteria*. New York, NY: Springer: 421–443. DOI: https://dx.doi.org/10.1007/978.[AQ4]

Lavaud, J, **Strzepek, R**, **Kroth, P.** 2007. Photoprotection capacity differs among diatoms: Possible consequences on the spatial distribution of diatoms related to fluctuations in the underwater light climate. *Limnology and Oceanography* **52**(3): 1188–1194. DOI: https://dx.doi.org/10.4319/lo.2007.52.3.1188.

Le Moigne, FA, **Poulton, AJ**, **Henson, SA**, **Daniels, CJ**, **Fragoso, GM**, **Mitchell, E**, **Richier, S**, **Russell, BC**, **Smith, HE**, **Tarling, GA**, **Young, JR**, **Zubkov, M**. 2015. Carbon export efficiency and phytoplankton community composition in the Atlantic sector of the Arctic Ocean. *Journal of Geophysical Research: Oceans* **120**(6): 3896–3912. DOI: https://dx.doi.org/10.1002/2015JC010700.

Lewis, K, **Arnsten, A**, **Coupel, P**, **Joy-Warren, H**, **Lowry, K**, **Matsuoka, A**, **Mills, M**, **van Dijken, GL**, **Selz, V**, **Arrigo, K.** 2018. Photoacclimation of Arctic Ocean phytoplankton to shifting light and nutrient limitation. *Limnology and Oceanography* **64**(1): 1–18. DOI: https://dx.doi.org/10.1002/lno.11039.

Lewis, K, **van Dijken, G**, **Arrigo, K.** 2020. Changes in phytoplankton concentration now drive increased Arctic Ocean primary production. *Science*

369(6500): 198–202. DOI: https://dx.doi.org/10.1126/science.aay8380.

Lewis, MR, **Smith, JC.** 1983. A small volume, short-incubation-time method for measurement of photosynthesis as a function of incident irradiance. *Marine Ecology Progress Series* **13**(1): 99–102.

Lovejoy, C, **Legendre, L**, **Martineau, MJ**, **Bâcle, J**, **Von Quillfeldt, C.** 2002. Distribution of phytoplankton and other protists in the North Water. *Deep Sea Research Part II: Topical Studies in Oceanography* **49**(22–23): 5027–5047. DOI: https://dx.doi.org/10.1016/S0967-0645(02)00176-5.

Lowry, K, **Pickart, R**, **Selz, V**, **Mills, M**, **Pacini, A**, **Lewis, K.** 2018. Under-ice phytoplankton blooms inhibited by spring convective mixing in refreezing leads. *Journal of Geophysical Research: Oceans* **123**(1): 90–109. DOI: https://dx.doi.org/10.1002/2016JC012575.

MacIntyre, HL, **Kana, TM**, **Anning, T**, **Geider, RJ.** 2002. Photoacclimation of photosynthesis irradiance response curves and photosynthetic pigments in microalgae and cyanobacteria. *Journal of Phycology* **38**(1): 17–38. DOI: https://dx.doi.org/10.1046/j.1529-8817.2002.00094.x.

MacIntyre, HL, **Kana, TM**, **Geider, RJ.** 2000. The effect of water motion on short-term rates of photosynthesis by marine phytoplankton. *Trends in Plant Science* **5**: 12–17. DOI: https://dx.doi.org/10.1016/S1360-1385(99)01504-6.

Mackey, M, **Mackey, D**, **Higgins, H**, **Wright, S.** 1996. CHEMTAX—A program for estimating class abundances from chemical markers: Application to HPLC measurements of phytoplankton. *Marine Ecology Progress Series* **144**: 265–283. DOI: https://dx.doi.org/10.3354/meps144265.

Martin, J, **Tremblay, JÉ**, **Gagnon, J**, **Tremblay, G**, **Lapoussière, A**, **Jose, C**, **Poulin, M**, **Gosselin, M**, **Gratton, Y**, **Michel, C.** 2010. Prevalence, structure and properties of subsurface chlorophyll maxima in Canadian Arctic waters. *Marine Ecology Progress Series* **412**: 69–84. DOI: https://dx.doi.org/10.3354/meps08666.

Maslanik, J, **Stroeve, J**, **Fowler, C**, **Emery, W.** 2011. Distribution and trends in Arctic sea ice age through spring 2011. *Geophysical Research Letters* **38**(13). DOI: https://dx.doi.org/10.1029/2011GL047735.

Massicotte, P, **Amiraux, R**, **Amyot, MP**, **Archambault, P**, **Ardyna, M**, **Arnaud, L**, **Artigue, L**, **Aubry, C**, **Ayotte, P**, **Bécu, G**, **Bélanger, S**, **Benner, R**, **Bittig, HC**, **Bricaud, A**, **Brossier, É**, **Bruyant, F**, **Chauvaud, L**, **Christiansen-Stowe, D**, **Claustre, H**, **Cornet-Barthaux, V**, **Coupel, P**, **Cox, C**, **Delaforge, A**, **Dezutter, T**, **Dimier, C**, **Domine, F**, **Dufour, F**, **Dufresne, C**, **Dumont, D**, **Ehn, J**, **Else, B**, **Ferland, J**, **Forget, M-H**, **Fortier, L**, **Galí, M**, **Galindo, V**, **Gallinari, M**, **Garcia, N**, **Ribeiro, CG**, **Gourdal, M**, **Gourvil, P**, **Goyens, C**, **Grondin, P-L**, **Guillot, P**, **Guilmette, C**, **Houssais, M-N**, **Joux, F**, **Lacour, L**, **Lacour, T**, **Lafond, A**, **Lagunas, J**, **Lalande, C**, **Laliberté, J**, **Lambert-Girard, S**, **Larivière, J**, **Lavaud, J**, **LeBaron, A**, **Leblanc, K**, **Gall, FL**, **Legras, J**, **Lemire, M**, **Levasseur, M**, **Leymarie, E**, **Leynaert, A**, **dos Santos, AL**, **Lourenço, A**, **Mah, D**, **Marec, C**, **Marie, D**, **Martin, N**, **Marty, C**, **Marty, S**, **Massé, G**, **Matsuoka, A**, **Matthes, L**, **Moriceau, B**, **Muller, P-E**, **Mundy, C-J**, **Neukermans, G**, **Oziel, L**, **Panagiotopoulos, C**, **Pangrazi, J-J**, **Picard, G**, **Picheral, M**, **du Sel, FP**, **Pogorzelec, N**, **Probert, I**, **Quéguiner, B**, **Raimbault, P**, **Ras, J**, **Rehm, E**, **Reimer, E**, **Rontani, J-F**, **Rysgaard, S**, **Saint-Béat, B**, **Sampei, M**, **Sansoulet, J**, **Schmechtig, C**, **Schmidt, S**, **Sempéré, R**, **Sévigny, C**, **Shen, Y**, **Tragin, M**, **Tremblay, J-É**, **Vaulot, D**, **Verin, G**, **Vivier, F**, **Vladoiu, A**, **Whitehead, J**, **Babin, M**. 2020. Green Edge ice camp campaigns: Understanding the processes controlling the under-ice Arctic phytoplankton spring bloom. *Earth System Science Data* **12**(1): 151–176. DOI: https://dx.doi.org/10.5194/essd-12-151-2020.

Maxwell, K, **Johnson, G.** 2000. Chlorophyll fluorescence—A practical guide. *Journal of Experimental Botany* **51**(345): 659–668. DOI: https://dx.doi.org/10.1093/jexbot/51.345.659.

Melling, H, **Gratton, Y**, **Ingram, G.** 2001. Ocean circulation within the North Water polynya of Baffin Bay. *Atmosphere-Ocean* **39**(3): 301–325. DOI: https://dx.doi.org/10.1080/07055900.2001.9649683.

Miller, LA, **Davelaar, M**, **Caleb, D**, **Mucci, A**, **Burgers, TM**, **Ahmed, M**, **Irish, V.** 2020. Dissolved inorganic carbon (DIC), total alkalinity, stable oxygen isotope (O-18), temperature, salinity, dissolved oxygen and other parameters measured from discrete samples and profile observations during the Canadian Coast Guard Ship Amundsen ArcticNet cruise (EXPOCODE 18DL20160603, Leg 1 and Leg 2) in the Eastern Canadian Arctic, Baffin Bay, Nares Strait, Lancaster Sound, Barrow Strait and Coronation Gulf from 2016-06-03 to 2016-08-23 (NCEI Accession 0217304) [subset used: Baffin Bay]. NOAA National Centers for Environmental Information. Dataset. Accessed September 11, 2020. DOI: https://dx.doi.org/10.25921/719e-qr37.

Mioduszewski, J, **Vavrus, S**, **Wang, M.** 2018. Diminishing Arctic sea ice promotes stronger surface winds. *Journal of Climate* **31**(19): 8101–8119. DOI: https://dx.doi.org/10.1175/JCLI-D-18-0109.1.

Moore, CM, **Suggett, DJ**, **Hickman, AE**, **Kim, YN**, **Tweddle, JF**, **Sharples, J**, **Geider, RJ**, **Holligan, PM.** 2006. Phytoplankton photoacclimation and photoadaptation in response to environmental gradients in a shelf sea. *Limnology and Oceanography* **51**(2): 936–949. DOI: https://dx.doi.org/10.4319/lo.2006.51.2.0936.

Nymark, M, **Valle, KC**, **Brembu, T**, **Hancke, K**, **Winge, P**, **Andresen, K**, **Johnsen, G**, **Bones, AM.** 2009. An integrated analysis of molecular acclimation to high light in the marine diatom *Phaeodactylum tricornutum*. *PLoS One* **4**(11): 1–14. DOI: https://dx.doi.org/10.1371/journal.pone.0007743.

Ohad, I, **Adir, N**, **Koike, H**, **Kyle, DJ**, **Inoue, Y.** 1990. Mechanism of photoinhibition *in vivo*. A reversible light-induced conformational change of reaction

center II is related to an irreversible modification of the D1 protein. *Journal of Biological Chemistry* **265**(4): 1972–1979. DOI: https://dx.doi.org/10.1016/S0021-9258(19)39927-2.

Ohad, I, **Kyle, D**, **Arntzen, C.** 1984. Membrane protein damage and repair: Removal and replacement of inactivated 32-kilodalton polypeptides in chloroplast membranes. *The Journal of Cell Biology* **99**(2): 481–485. DOI: https://dx.doi.org/10.1083/jcb.99.2.481.

Pabi, S, **van Dijken, GL**, **Arrigo, KR.** 2008. Primary production in the Arctic Ocean, 1998–2006. *Journal of Geophysical Research: Oceans* **113**(C8). DOI: https://dx.doi.org/10.1029/2007JC004578.

Palmer, MA, **Arrigo, KR**, **Mundy, C**, **Ehn, JK**, **Gosselin, M**, **Barber, DG**, **Martin, J**, **Alou, E**, **Roy, S**, **Tremblay, JÉ.** 2011. Spatial and temporal variation of photosynthetic parameters in natural phytoplankton assemblages in the Beaufort Sea, Canadian Arctic. *Polar Biology* **34**(12): 1915–1928. DOI: https://dx.doi.org/10.1007/s00300-011-1050-x.

Palmer, MA, **van Dijken, GL**, **Mitchell, BG**, **Seegers, BJ**, **Lowry, KE**, **Mills, MM**, **Arrigo, KR.** 2013. Light and nutrient control of photosynthesis in natural phytoplankton populations from the Chukchi and Beaufort seas, Arctic Ocean. *Limnology and Oceanography* **58**(6): 2185–2205. DOI: https://dx.doi.org/10.4319/lo.2013.58.6.2185.

Peralta-Ferriz, C, **Woodgate, RA.** 2015. Seasonal and interannual variability of pan-Arctic surface mixed layer properties from 1979 to 2012 from hydrographic data, and the dominance of stratification for multiyear mixed layer depth shoaling. *Progress in Oceanography* **134**: 19–53. DOI: https://dx.doi.org/10.1016/j.pocean.2014.12.005.

Perrette, M, **Yool, A**, **Quartly, G**, **Popova, EE.** 2011. Near-ubiquity of ice-edge blooms in the Arctic. *Biogeosciences* **8**(2): 515. DOI: https://dx.doi.org/10.5194/bg-8-515-2011.

Platt, T, **Gallegos, CL**, **Harrison, WG.** 1980. Photoinhibition of photosynthesis in natural assemblages of marine phytoplankton. *Journal of Marine Research* **38**: 687–701.

Platt, T, **Harrison, W**, **Irwin, B**, **Horne, EP**, **Gallegos, CL.** 1982. Photosynthesis and photoadaptation of marine phytoplankton in the Arctic. *Deep Sea Research Part A Oceanographic Research Papers* **29**(10): 1159–1170. DOI: https://dx.doi.org/10.1016/0198-0149(82)90087-5.

Randelhoff, A, **Oziel, L**, **Massicotte, P**, **Bécu, G**, **Gali, M**, **Lacour, L**, **Dumont, D**, **Vladoiu, A**, **Marec, C**, **Bruyant, F**, **Houssais, MN**, **Tremblay, JÉ**, **Deslongchamps, G**, **Babin, M.** 2019. The evolution of light and vertical mixing across a phytoplankton ice-edge bloom. *Elementa: Science of the Anthropocene* **7**(20). DOI: https://dx.doi.org/10.1525/elementa.357.

Ras, J, **Claustre, H**, **Uitz, J.** 2008. Spatial variability of phytoplankton pigment distributions in the Subtropical South Pacific Ocean: Comparison between in situ and predicted data. *Biogeosciences* **5**(2). DOI: https://dx.doi.org/10.5194/bg-5-353-2008.

Sakshaug, E, **Demers, S**, **Yentsch, C**. 1987. *Thalassiosira oceanica* and *T. pseudonana*: Two different photoadaptational responses. *Marine Ecology Progress Series* **41**(3): 275–282. Available at https://www.jstor.org/stable/24827436.

Smith, R, **Prézelin, B**, **Baker, K**, **Bidigare, R**, **Boucher, N**, **Coley, T.** 1992. Ozone depletion: Ultraviolet radiation and phytoplankton biology in Antarctic. *Science* **255**(5047): 952–959. DOI: https://dx.doi.org/10.1029/2010JC006553.[AQ5]

Stramski, D, **Reynolds, RA**, **Kaczmarek, S**, **Uitz, J**, **Zheng, G.** 2015. Correction of pathlength amplification in the filter-pad technique for measurements of particulate absorption coefficient in the visible spectral region. *Applied Optics* **54**(22): 6763–6782. DOI: https://dx.doi.org/10.1364/AO.54.006763.

Stroeve, J, **Holland, MM**, **Meier, W**, **Scambos, T**, **Serreze, M.** 2007. Arctic sea ice decline: Faster than forecast. *Geophysical Research Letters* **34**(9). DOI: https://dx.doi.org/10.1029/2007GL029703.

Stroeve, J, **Notz, D**. 2018. Changing state of Arctic sea ice across all seasons. *Environmental Research Letters* **13**(10): 103001. DOI: https://dx.doi.org/10.1088/1748-9326/aade56.

Suggett, DJ, **Moore, CM**, **Hickman, AE**, **Geider, RJ.** 2009. Interpretation of fast repetition rate (FRR) fluorescence: Signatures of phytoplankton community structure versus physiological state. *Marine Ecology Progress Series* **376**: 1–19. DOI: https://dx.doi.org/10.3354/meps07830.

Tang, CC, **Ross, CK**, **Yao, T**, **Petrie, B**, **DeTracey, BM**, **Dunlap, E.** 2004. The circulation, water masses and sea-ice of Baffin Bay. *Progress in Oceanography* **63**(4): 183–228. DOI: https://dx.doi.org/10.1016/j.pocean.2004.09.005.

Tremblay, JÉ, **Gratton, Y**, **Carmack, EC**, **Payne, CD**, **Price, NM.** 2002. Impact of the large-scale Arctic circulation and the North Water Polynya on nutrient inventories in Baffin Bay. *Journal of Geophysical Research: Oceans* **107**(C8): 1–6. DOI: https://dx.doi.org/10.1029/2000JC000595.

Tremblay, JÉ, **Hattori, H**, **Michel, C**, **Ringuette, M**, **Mei, ZP**, **Lovejoy, C**, **Fortier, L**, **Hobson, KA**, **Amiel, D**, **Cochran, K.** 2006. Trophic structure and pathways of biogenic carbon flow in the eastern North Water Polynya. *Progress in Oceanography* **71**(2–4): 402–425. DOI: https://dx.doi.org/10.1016/j.pocean.2006.10.006.

Tremblay, JÉ, **Simpson, K**, **Martin, J**, **Miller, L**, **Gratton, Y**, **Barber, D**, **Price, NM.** 2008. Vertical stability and the annual dynamics of nutrients and chlorophyll fluorescence in the coastal, southeast Beaufort Sea. *Journal of Geophysical Research: Oceans* **113**(C7). DOI: https://dx.doi.org/10.1029/2007JC004547.

Van Kooten, O, **Snel, J.** 1990. The use of chlorophyll fluorescence nomenclature in plant stress physiology. *Photosynthesis Research* **25**: 147–150.

Van Leeuwe, M, **Visser, R**, **Stefels, J.** 2014. The pigment composition of *Phaeocystis antarctica* (Haptophyceae) under various conditions of light, temperature, salinity, and iron. *Journal of Phycology* **50**: 1070–1080. DOI: https://dx.doi.org/10.1111/jpy.12238.

Wang, M, **Overland, JE.** 2009. A sea ice free summer Arctic within 30 years? *Geophysical Research Letters* **36**(7). DOI: https://dx.doi.org/10.1029/2009GL037820.

Wassmann, P, **Bauerfeind, E**, **Fortier, M**, **Fukuchi, M**, **Hargrave, B**, **Moran, B**, **Noji, T**, **Nöthig, EM**, **Olli, K**, **Peinert, R**, **Sasaki, H**, **Shevchenko, V**. 2004. Particulate organic carbon flux to the Arctic Ocean sea floor, in Stein, R, MacDonald, RW eds., *The organic carbon cycle in the Arctic Ocean*. Berlin, Germany: Springer: 101–138. DOI: https://dx.doi.org/10.1007/978-3-642-18912-8_5.

Wassmann, P, **Duarte, CM**, **Agusti, S**, **Sejr, MK.** 2011. Footprints of climate change in the Arctic marine ecosystem. *Global Change Biology* **17**(2): 1235–1249. DOI: https://dx.doi.org/10.1111/j.1365-2486.2010.02311.x.

How to cite this article: Joy-Warren, H, Lewis, KM, Ardyna, M, Tremblay J-É, Babin, M, Arrigo KR. 2022. Similarity in phytoplankton photophysiology among under-ice, marginal ice, and open water environments of Baffin Bay (Arctic Ocean). *Elementa: Science of the Anthropocene* 11(1). DOI: https://doi.org/10.1525/elementa.2021.00080

Domain Editor-in-Chief: Jody W. Deming, University of Washington, Seattle, WA, USA

Associate Editor: Christine Michel, Department of Fisheries and Oceans, University of Manitoba, Winnipeg, Canada

Knowledge Domain: Ocean Science

Part of an Elementa Special Feature: Green Edge

Published: 00, 0000 **Accepted:** February 28, 2023 **Submitted:** September 16, 2021

ELEMENTA Science of the Anthropocene

Elem Sci Anth is a peer-reviewed open access journal published by University of California Press.

OPEN ACCESS

Author Query Form

Please respond to and approve your proof through the "Edit" tab, using this PDF to review figure and table formatting and placement. This PDF can also be downloaded for your records. We strongly encourage you to provide any edits through the "Edit" tab, should you wish to provide corrections via Kitaboo Edit.

Journal Title: ELEMENTA

No.	Query
	Please confirm that all author information, including names, affiliations, sequence, and contact details, is correct.
	Please review the entire document for typographical errors, mathematical errors, and any other necessary corrections; check headings, tables, and figures.
	Please ensure that you have obtained and enclosed all necessary permissions for the reproduction of artistic works, (e.g., illustrations, photographs, charts, maps, other visual material, etc.) not owned by yourself. Please refer to your publishing agreement for further information.
	Please confirm that the Funding and Conflict of Interest statements are accurate.
	Please note that this proof represents your final opportunity to review your article prior to publication, so please do send all of your changes now.
AQ: 1	Author initials "HLJW" is set as "HJW' to match the author name in the author byline.
AQ: 2	Please provide accessed date for Ref. "Arctic Monitoring and Assessment Programme. 2017."
AQ: 3	Please insert accessed date for Ref. Intergovernmental Panel on Climate Change. 2019.
AQ: 4	Please provide an appropriate URL and editor name(s) for the Ref. "Lavaud, J, Goss, R. 2014."
AQ: 5	Please provide an appropriate URL for Ref. "Smith, R, Prézelin, B, Baker, K, Bidigare, R, Boucher, N, Coley, T. 1992," as it does not match with the article title provided.